Image Cover Sheet

CLASSIFICATION	SYSTEM NUMBER
UNCLASSIFIED	154344

TITLE

A SHIPBORNE SURVEILLANCE RADAR MODEL FOR DATA FUSION STUDIES

System Number:

Patron Number:

Requester:

Notes:

DSIS Use only:

Deliver to: FF

UNCLASSIFIED

DEFENCE RESEARCH ESTABLISHMENT
CENTRE DE RECHERCHES POUR LA DÉFENSE
VALCARTIER, QUÉBEC

DREV - R - 9429
Unlimited Distribution / Distribution illimitée

A SHIPBORNE SURVEILLANCE RADAR MODEL FOR DATA FUSION STUDIES

by

É. Bossé, D. Dion and J. Roy

November / novembre 1995

Approved by / approuvé par

Director / Directeur

11/10/95

Date

SANS CLASSIFICATION

ABSTRACT

This report presents a surveillance radar model to support the ongoing Multi-Sensor Data Fusion performance evaluation study for potential application to the Canadian Patrol Frigate midlife upgrade. This surveillance radar model takes into account the sensor's design parameters and external environmental effects such as clutter, propagation and jamming. To a large extent, the model is based on the available literature and on relevant experience and recent studies in the field. In addition, the latest findings regarding the dominant perturbing effects affecting the radar detection performance are included. The radar model can be used to generate contacts and false alarms in scenarios for multi-sensor data fusion studies while the scenario is running.

RÉSUMÉ

Ce document présente un modèle de radar de surveillance pour appuyer une étude en cours portant sur l'évaluation de la performance de la fusion de données multi-capteurs pour une application éventuelle pour la modernisation de la Frégate de patrouille canadienne. Le modèle tient compte des paramètres du capteur proprement dit et des effets de l'environment tels le fouillis de mer, la propagation et le brouillage. Le modèle s'appuie en large partie sur la documentation disponible, mais incorpore les récentes connaissances relatives aux effets les plus perturbants affectant la détection radar. Le modèle est approprié pour des études en fusion de données qui nécessistent la génération de vrais contacts et de fausses alertes durant l'exécution d'un scénario donné.

TABLE OF CONTENTS

EXECUTIVE SUMMARY

A major ongoing activity undertaken by the Data Fusion Group in the Command and Control Division at Defence Research Establishment Valcartier (DREV) is to explore sensor management, integration, and data fusion concepts that could be applied to the current Canadian Patrol Frigate (CPF) Above Water Warfare (AWW) sensor suite, as well as its possible future upgrades, in order to improve its performance against current and future threats. The approach retained for this activity is to employ sufficiently representative sensor and phenomenological simulators.

This report presents a surveillance radar model to support an ongoing Multi-Sensor Data Fusion (MSDF) performance evaluation study for potential applications to the Canadian Patrol Frigate midlife upgrade. This surveillance radar model takes into account the sensor's design parameters and external environmental effects such as clutter, propagation and jamming. The latest findings regarding the dominant perturbing effects affecting the radar detection performance are included. In addition, the radar model can be used to generate contacts and false alarms in scenarios for multi-sensor data fusion studies while the scenario is running.

The radar simulation provides a "realistic" representation of a radar behavior in typical operational environments. A panoramic pulse-MTI/Doppler search radar, typical of the Canadian Navy surveillance radars, using a rotating antenna that scans 360 degrees in azimuth is considered. The scenarios of interest consist of point-target (missiles) attacks in an open-sea environment. The proposed model is more versatile and more generally applicable than those published so far; it considers a wider range of parameters which affect a search or surveillance radar's performance. It is therefore likely to yield more realistic results.

The results of this research are of prime importance when considering mid-life update of the Canadian Patrol Frigate.

LIST OF ACRONYMS

AAW	Anti-Air Warfare
AWW	Above Water Warfare
C^2	Command and Control
CARPET	Computer-Aided Radar Performance Evaluation Tool
CASE_ATTI	Concept Analysis and Simulation Environment for Automatic Target Tracking and Identification
CCS	C^2 System
CFAR	Constant False Alarm Rate
CPF	Canadian Patrol Frigate
CRDV	Centre de recherches pour la défense, Valcartier
DFT	Discrete Fourier Transform
DREV	Defence Research Establishment Valcartier
E-O	Electro-Optical
ESM	Electronic Support Measure
EREPS	Engineer's Refractive Effects Prediction Software
FFT	Fast Fourier Transform
FIR	Finite Impulse Response
GIT	Georgia Institute of Technology
HP	Horizontal Polarization
IF	Intermediate Frequency
MBL	Marine Boundary Layer
MSDF	Multi-Sensor Data Fusion
MTI	Moving Target Indicator
PEM	Parabolic Equation Method
PRF	Pulse Repetition Frequency
RCS	Radar Cross Section
RF	Radio Frequency
RPM	Revolution Per Minute
SURSEM	Surveillance Radar Systems Evaluation Model
VP	Vertical Polarization
WKD	Wamsley KEL DREV

LIST OF SYMBOLS

SYMBOLS RELATED TO RADAR INPUTS

P_t: transmitted pulse power (w)

G: maximum antenna gain

F_j: one-way propagation factor for jamming signal

$L_{t/r}$: transmit/receive losses

L_r: receive loss (taken to be 1/2 $L_{t/}$)

f : frequency in (GHz)

λ: wavelength (m)

h_a: antenna height (m)

θ_b: horizontal 3 dB beamwidth (rad)

L_{sl}: azimuth sidelobe radar antenna level with respect to main beam

N_{fc}: number of pulses before a frequency change

N_{pc}: order of the MTI filter (N_{pc}-pulse canceler)

$K_{clutter}$: clutter false alarm factor

t_{fa}: mean time between false alarms (s)

t_{scan} : time of one radar revolution (s)

N_{ch}: number of radar decision channels

f_r: pulse repetition frequency (Hz)

τ' : the compressed pulse width (s)

N_f: receiver noise figure (RF preamplifier, mixer, IF amplifiers)

N_c: number of pulse coherently integrated

P_{facmax}: maximum horizontal polarization clutter false alarm probability (suggested value between 10^{-2} and 10^{-3})

SYMBOLS RELATED TO INPUT ENVIRONMENTAL PARAMETERS

h_{cloud}: height of the cloud base (height of the rain volume) (m)

p_r : precipitation rate (mm/hr)

w_h : *significant* wave height (m)

h_e: effective wave height (m), ($0.375w_h$)

h_{duct}: duct height (m)

S_{sea} : sea-state number (Douglas scale)

w_s : wind speed in (m/s)

SYMBOLS RELATED TO INTERMEDIATE PARAMETERS

R or R_S: slant range to the target (m)

R_t: terrestrial range of the target (m)

g : antenna directivity factor (function of azimuth and elevation)

F: propagation factor

C_R : range cell width (m)

N_{rc}: number of range cells

T_s : system noise temperature (K)

B_N : noise bandwidth of the receiver (Hz)

N_0': thermal noise power at the output of the IF stage (W)

K_r : radar constant, $K_r = \dfrac{P_t G^2 \lambda^2}{(4\pi)^3 L_{t/r} L_{atm}^2}$

f_d: Doppler frequency (Hz)

G_p: processing gain of the video stage

N_e: number of pulses available for the non-coherent integration

σ: computed target cross section (m^2)

σ_n: nose-on cross section (m^2) (input)

ϕ': elevation angle between the line of sight and the target speed vector (rad)

θ': bearing angle between the line of sight and the target speed vector (rad)

L: length of the missile target (m) (input)

D: diameter of the missile target (m) (input)

m : modified refractive index which accounts for the earth's curvature

n : refractive index

r : earth radius (m)

R_{sc} : slant range of the illuminated patch in the case of sea-clutter (m)

A : area of the illuminated sea patch (m^2), ($A = R_{sc}\theta_b C_R$)

σ_0* : reflectivity of the sea surface per unit area in the cell (m^2 / m^2)

σ_0^{50}: median reflectivity (m^2/m^2)

P_{sc} : mean power received from sea backscatters (W)

σ_s: standard deviation of the sea-clutter spectrum (Hz)

σ_{wc}: standard deviation of weather-clutter spectrum (Hz)

μ_c: mean of the sea-clutter spectrum (Hz)

P_{WC}: power received from weather clutter at the input of the receiver (W)

ϑ_0 : weather clutter reflectivity (m^2/m^3),

ϑ: weather clutter cross-section (m^2)

d_h : height of the volume cell (m)

L_{atm}: atmospheric loss (oxygen, water vapor absorption and rain attenuation)

L_{wo}: losses caused by oxygen and water vapor absorption

L_d: clutter distribution loss (for non-Rayleigh clutter)

L_{cd} : clutter distribution sensitivity loss (for non-Rayleigh clutter)

$\gamma_{f/c}$: attenuation coefficient (dB/km) caused by fog or clouds

γ_r: attenuation coefficient (dB/km) caused by rain or snow

γ_{ic}: attenuation coefficient (dB/km) caused by ice clouds

P_j: power of the jamming (W)

P_{jt}: transmitted jammer power (W)

G_j: jammer antenna gain

B : radar bandwidth for the calculation of the signal-to-jamming ratio (Hz)

R_j: jammer range (m)

B_j: jammer bandwidth (Hz)

ε_R: computed mean range measurement error (m)

ε_θ: computed mean azimuth measurement error (rad)

R_{meas}: measured target range (m)

θ_{meas}: measured target azimuth (rad)

P_{fac}: probability of sea-clutter false alarm

1.0 INTRODUCTION

A major ongoing activity undertaken by the Data Fusion Group in the Command and Control Division at Defence Research Establishment Valcartier (DREV) is to explore sensor management, integration, and data fusion concepts that could apply to the current Canadian Patrol Frigate (CPF) Above Water Warfare (AWW) sensor suite, as well as its possible future upgrades, in order to improve its performance against current and future threats. The approach retained for the activity is to employ sufficiently representative sensor and phenomenological simulations. To achieve this capability, a highly modular, structured, and flexible simulation environment has been developed.

DREV's Concept Analysis and Simulation Environment for Automatic Target Tracking and Identification (CASE_ATTI) (Ref. 1) provides the algorithm-level test and replacement capability required to study and compare the applicability and performance of advanced, state-of-the-art Multi-sensor Data Fusion (MSDF) techniques. The CASE_ATTI system allows the user to create and edit multi-sensor multi-target test scenarios. A typical scenario consists of platforms (e.g., ships) with sensors, and targets. The platforms can be stationary or moving along predefined paths. One or several sensors (potentially dissimilar such as radar, infrared, ESM, etc.) can be assigned to each platform. Targets are created with defined trajectories and attributes. The scenario also allows for the selection of environmental conditions that may affect the various sensor detection performance and measurements accuracy.

The CASE_ATTI tool comprises three major modules, as shown in Fig.1. The sensor module is responsible for providing realistic measurement data to the tracking module. This module also offers the ability to integrate real sensor data into the simulation. The tracking module supports a wide variety of fusion architectures, varying from a simple single sensor tracker to an arbitrarily complex hierarchical multiple-sensor

topology. The graphics module provides the tools to examine the tracking performance and the results of the sensor fusion. The object-oriented design allows the users to easily develop and incorporate their own tracking algorithms, sensor models, and analysis tools.

This report presents a surveillance radar model for the CASE_ATTI sensor module. A thorough demonstration of its validity under various threat and environmental conditions will be presented shortly in a follow-up report, emphasizing the case of current Canadian Navy radars. This surveillance radar model takes into account the sensor's design parameters and external environmental effects such as clutter, propagation (multipath and refraction) and jamming. To a large extent the model is based on the available literature and recent studies in the field. In addition, the latest findings regarding the dominant perturbing effects affecting the radar detection performance are included in the simulation.

A requirement for data fusion studies is that the radar model can be used to generate contacts and false alarms in scenarios for multi-sensor data fusion studies while the scenario is running. Recent surveillance radar simulations, such as CARPET (Ref. 2) and previous ones (Refs. 3-4), are not fully suitable for sensor fusion studies mainly because of this requirement. CARPET only gives plots of radar detection probability versus range as well as plots of intermediate results (or dependent parameters), such as MTI (Moving Target Indicator), improvement factor and propagation loss. The results provided by CARPET are not available as numerical data and this prevents their use in the CASE_ATTI tool.

The model proposed here is made of two levels of processing: off-line and on-line. At the first level, various software modules are provided to precompute tables that represent the dominant perturbing effects on the radar detection. At the second level, which resides in CASE_ATTI, the probability of detection (P_d) is evaluated using the tables each time a target meets the radar beam. Measurements are then generated

according to the P_d and the signal-to-interference ratio. In addition, the simulation generates false alarms as caused by clutter and system noise.

The radar model provides a realistic representation of a radar behavior in typical operational environments. A panoramic pulse-MTI/Doppler search radar, typical of Canadian Navy surveillance radars, using a rotating antenna that scans 360 degrees in azimuth is considered. The scenarios of interest consist of point-targets (missiles) attacks in an open-sea environment. The proposed model is more flexible and more generally applicable than those (Refs. 2-4) published so far; it considers a wider range of parameters which affect search or surveillance radar performances. It is therefore likely to yield more realistic results. In particular, this model brings the following features:

- extension of sea-clutter models to account for ducting;
- better identification of the various losses of typical surveillance radars;
- full Parabolic Equation Method (PEM) computation of the propagation factor;
- a model to generate false alarms induced by sea clutter;
- a flexible and generic model to represent the effects of signal processing;
- a simulation architecture allowing refinement in modeling as well as real-time use for data fusion studies.

This document is organized as follows. Chapter 2 gives a general description of the radar model. Chapter 3 presents the calculations of the target signal power and the receiver noise. In Chapter 4, the interfering signals from clutter and jamming are discussed. Chapter 5 addresses the radar signal processing issues. Chapter 6 and 7 show how the target contacts and false alarms are generated. Finally, Chapter 8 ends up with the conclusion.

This work was carried out at DREV between 1992 and 1994 under PSC 12C, Ship Combat System Integration.

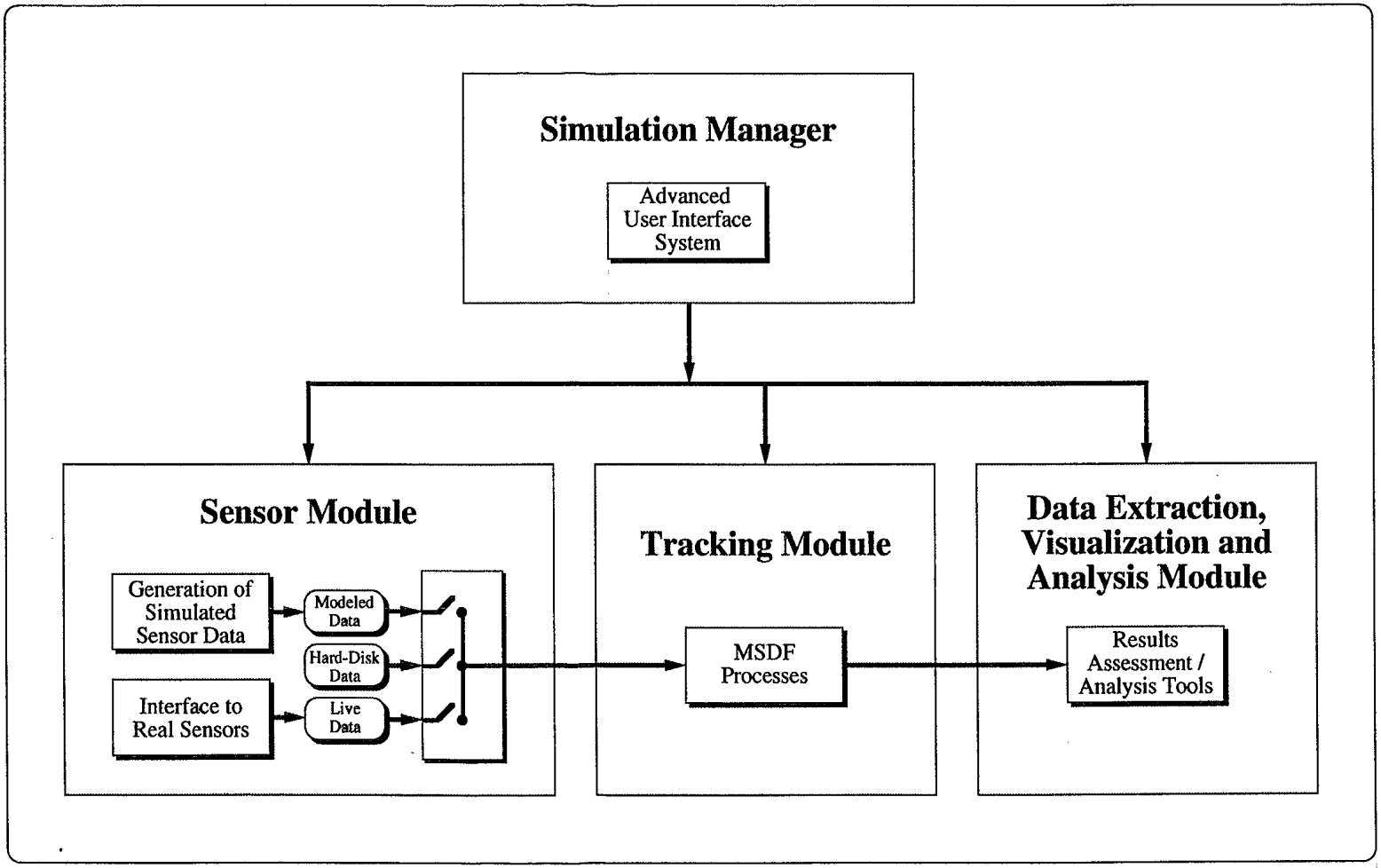

FIGURE 1 - CASE_ATTI global structure

2.0 GENERAL DESCRIPTION OF THE RADAR MODEL

The search process consists in scanning a volume of space and reporting detections within the volume. Detections are declared when the signal received and processed exceeds a threshold. These detections can be due to the presence of real targets (true detections) in the volume or due to noise or returns from objects that are not targets (false alarms).

A panoramic pulse-MTI/Doppler search radar, typical of the Canadian Navy surveillance radars, using a rotating antenna that scans 360 degrees in azimuth is considered. The operation of a typical pulse radar receiver can be described with the aid of the block diagram shown in Fig. 2.

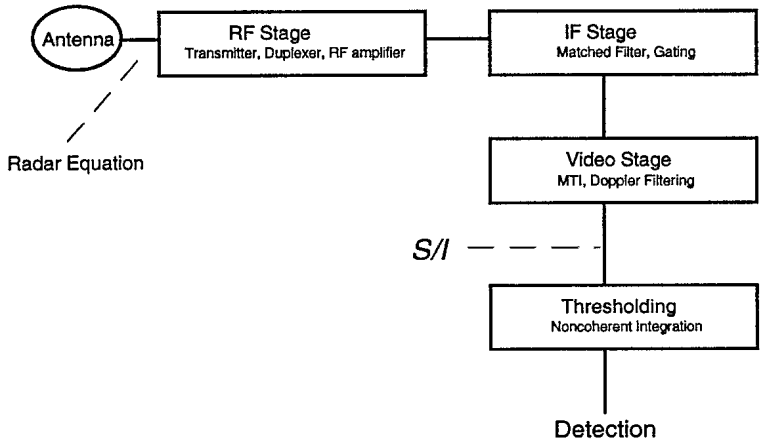

FIGURE 2 - Block diagram of a pulse radar

A single antenna (and its lines/waveguides) is generally used for both transmitting and receiving via a duplexer. The receiver is usually made of a low-noise RF amplifier

an Intermediate Frequency (IF). The IF amplifier is designed as a matched filter to maximize the signal-to-noise ratio. The IF signal is further down converted to video where signal processing can be more conveniently applied.

The surveillance radar model takes into account not only the sensor's design parameters but also the determinant factors affecting detection such as clutter, multipath, ducting, and the signal processing gain of the radar-environment-target chain by considering a Signal-to-Interference ratio (*S/I*):

$$\frac{S}{I} = \frac{S}{N_0 + C + J} \qquad [1.]$$

where N_0, C, and J are the energy from system noise, clutter and jamming, respectively. In the simulation, the *S/I* is approximated by finding the dominant interference: N_0, C or J. In our model, when these three sources of interference are competing, clutter is taken as being the dominant one.

The *S/I* is used to evaluate the probability of detection, P_d, each time a target is geometrically hit by the radar beam. Measurements of range and azimuth of each target are then generated according to P_d and *S/I*. In addition, the simulation generates measurements (range and azimuth) corresponding to false alarms caused by clutter and system noise.

The proposed model (Fig. 3) has two levels of processing. At the first level, called *off-line processing level*, software modules have been developed to precompute tables giving the critical parameters required to calculate the *S/I*. These parameters require extensive computations; furthermore, these external modules can be conveniently upgraded as improved models become available. At the second level, called *on-line processing level*, which resides within the CASE_ATTI sensor module, the *S/I* is computed and the probability of detection (P_d) is evaluated each time a target meets the radar beam. The two-level processing architecture provides the flexibility of using various

non-standardized pieces of software to precompute sensitive parameters without increasing the complexity and the execution speed of CASE_ATTI.

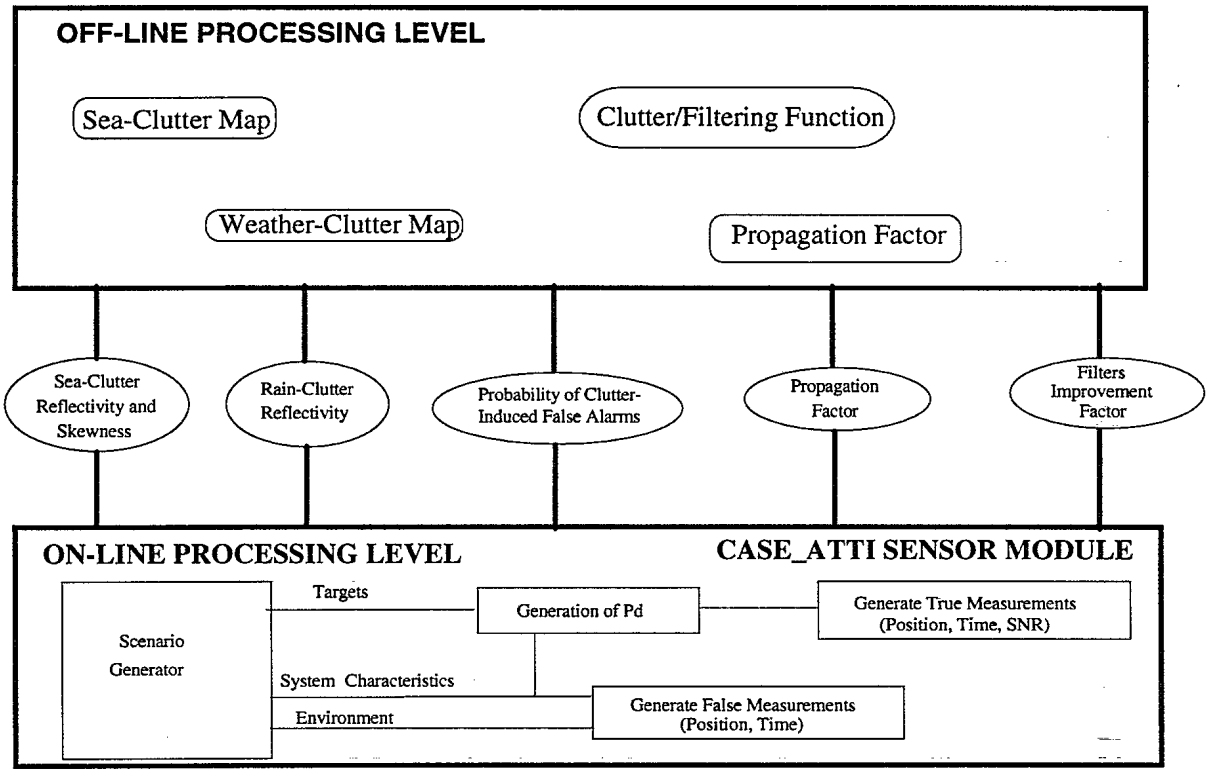

FIGURE 3 - Block diagram of the surveillance radar simulation

2.1 Off-Line Processing Level

For various sets of weather conditions and radar characteristics, tables are computed outside CASE_ATTI to provide parameters or coefficients for the computation of:

- sea-clutter power and skewness;
- weather-clutter power;
- propagation factor;

- filters improvement factor;
- clutter-induced probability of false alarms.

Coefficients for *sea- and weather-clutter reflectivities* are calculated versus range and azimuth. For sea clutter, classical models have been extended to incorporate ducting effects. The extensions are based on data recently published. In addition, the *skewness of the statistical distribution of the sea clutter* is estimated and described by a factor and the *probability of false alarms induced by sea clutter* is also estimated. The *propagation factor* represents the interference pattern as due to multipath, taking into account refraction effects. It is computed using the Parabolic Equation Method (PEM) (Ref. 5). The filter *improvement factor* is used to compute the efficiency of clutter rejection of Moving Target Indicator (MTI) and Doppler filters. Tables of the filter improvement factors versus the standard deviation of the Gaussian clutter spectrum and the target Doppler shift are produced. The standard deviation and the target Doppler shift are both normalized to the Pulse Repetition Frequency (f_r). Various kind of Doppler filtering processes are supported: N-pulse canceler, N-pulse Doppler-filter bank, cascade of MTI to a Doppler filter-bank. Filter sidelobe reduction can also be provided by applying Taylor, Chebyshev, Hamming or Hann windowing.

2.2 On-Line Processing Level

In the CASE_ATTI sensor module, the precomputed parameters are used to evaluate P_d each time a target is geometrically hit by the radar beam and to generate false detections. Of course, to run a scenario in CASE_ATTI the required precomputed tables for the selected sensors and environmental conditions must be available.

2.2.1 Target Detection

Each time the beam hits a target, the target's probability of detection P_d is computed taking into account the radar parameters and the environmental effects. Calculations are made for the resolution cell that contains the target. If more than one target happen to be in the same "resolution" cell, the program checks if the targets can be differentiated by the Doppler filters. The signal power received from all non-differentiated targets is added. The result constitutes "the desired target signal".

Conceptually, the *S/I* at the output of the video stage has to be computed, and at the detector module (thresholding), the corresponding P_d has to be evaluated. When a detection is declared, the radar model outputs the following parameters:

- target range (km);
- target azimuth (deg-true north);
- signal-to-interference ratio, *S/I* (dB)

2.2.2 False Alarm Generation

In any radar system, a device called the CFAR (Constant False Alarm Rate) is used to maintain the prescribed false alarm rate constant. This device comprises a processor which samples and processes the interfering signal in the radar cells to estimate the noise level and dynamically adjust the detection threshold to maintain a fixed P_{fa} (probability of false alarm) based on estimates of interference statistics.

Noise-induced false alarms are generated randomly at a rate corresponding to the false alarm rate given by the user. The relationship between P_{fa} and the false alarm rate (r_{fa}) depends on the radar characteristics. In addition, further false detections can be generated due to the spiky nature of sea clutter. Most radar simulations have exclusively regarded the evaluation of target probability of detection in noise/clutter, and the current knowledge of clutter is not sufficiently advanced to provide an accurate representation of

clutter-produced false alarm outcomes. We choose to use heuristic methods to achieve a likely spreading of false alarms as a function of radar characteristics and the environment. A probability of false alarms, P_{fac} is estimated as a function of range and azimuth. Details on the technique are given in Chapter 7.

3.0 TARGET SIGNAL POWER AND RECEIVER NOISE

This section aims at computing the signal-to-noise ratio at the output of the IF stage.

3.1 Target Signal Power

The power received at the input of the RF stage (Fig. 2) from a single-target echo is given by

$$P_r = K_r \frac{\sigma F^4}{R^4} \qquad [2.]$$

with

$$K_r = \frac{P_t G^2 \lambda^2}{(4\pi)^3 L_{t/r} L_{atm}^2} \qquad [3.]$$

where

P_t: transmitted pulse power (w),

G: maximum antenna gain,

F: propagation factor,

σ: target cross section (m^2),

$L_{t/r}$: transmit/receive losses,

L_{atm}: atmospheric loss (oxygen, water vapor absorption and rain attenuation),

R: target range (m),

λ: wavelength (m).

3.1.1 Transmit/Receive Losses

The total transmit/receive system loss, $L_{t/r}$, is the product of numerous individual loss factors from the output of the transmitter to the antenna. Among them are the loss in transmission lines, the radome loss, the loss in connectors and the attenuation when the

signal passes the duplexer (insertion loss). It is the responsibility of the user to estimate the various contributions and to input the resulting loss in the radar specifications.

3.1.2 Propagation Factor

The propagation factor F accounts for the radar wave propagation effects resulting from non-free-space conditions. It includes the combined effects of refraction (bending of rays), multipath, as due to earth reflections, and antenna gain directivity $g(\phi)$ (discussed in Section 3.1.3). The basic definition of the propagation factor is:

$$F = \left| \frac{E}{E_0} \right| \qquad [4.]$$

where E is the actual intensity of the electric field impinging on a target at distance R from the source, while E_0 is the field that would exist at the target range in free space with the target in the direction of the maximum antenna gain.

To perform field strength calculations, the use of the parabolic approximation of the elliptic scalar wave Helmoltz equation, commonly known as Parabolic Equation Method (PEM), has received wide acceptance in recent years (Refs. 5-6). The PEM approach applies a full-wave, forward-scatter model capable of predicting propagation for arbitrary atmospheric refractivities. In the PEM, the field is expressed in terms of a complex electrical field attenuation function in space, $u(R_t, h)$ (V/m$^{1/2}$):

$$\frac{\partial^2 u}{\partial h^2} + 2j\kappa \frac{\partial u}{\partial R_t} + \kappa^2 (m^2(R_t, h) - 1)u = 0 \qquad [5.]$$

where κ is the free-space wave number, R_t is the terrestrial range and h is the height above the surface. The modified refractive index, m, accounts for the earth's curvature ($m = n + h/r$) where n is the refractive index and r the earth radius. The propagation factor is related to u by:

$$F = |u(R_t, h)|\sqrt{R_t} \qquad [6.]$$

A recently developed implementation of the split-step Fourier technique is used to solve [5] (Ref. 6). The calculation requires as inputs: radar frequency and polarization, antenna height (above the sea surface), antenna directivity pattern, sea-wave height and refractive index of air. Arbitrary vertical profiles of m can be user-defined. Otherwise, the following common default profile is used:

$$m(h) = 1 + \left(M_0 + 0.125\left(h - h_{duct} \log\left(h/z_0 \right) \right) \right) \times 10^{-6} \qquad [7.]$$

where the evaporation duct height is h_{duct}(m), M_0 is the surface modified refractivity (made equal to 320 M units) and z_0 is the roughness length equal to 1.5 x 10^{-4} m. The duct height is calculated from the air temperature and humidity, the wind speed and the water temperature using the marine boundary layer model Wamsley-KEL-DREV (WKD) (Ref. 7).

Figure 4 shows the effects of ducting on the propagation factor against range. Cases of duct heights of 0, 5, 10 and 15 m are shown. The target height and the antenna height are 25 m and 20 m, respectively. We observe that nulls move right as a function of duct height and the null displacement becomes significant at ranges as close as 5 km.

As mentioned in Chapter 2, the propagation factor values are precomputed in the space domain (R_t, h) for specific radar and environmental parameter inputs. In a simulation run, when a table is missing or a requested coordinate is located outside the (R_t, h) domain of the supplied table, a standard multipath factor calculation is performed, as detailed in Ref. 8. It is the responsibility of the simulation-user to provide the necessary table.

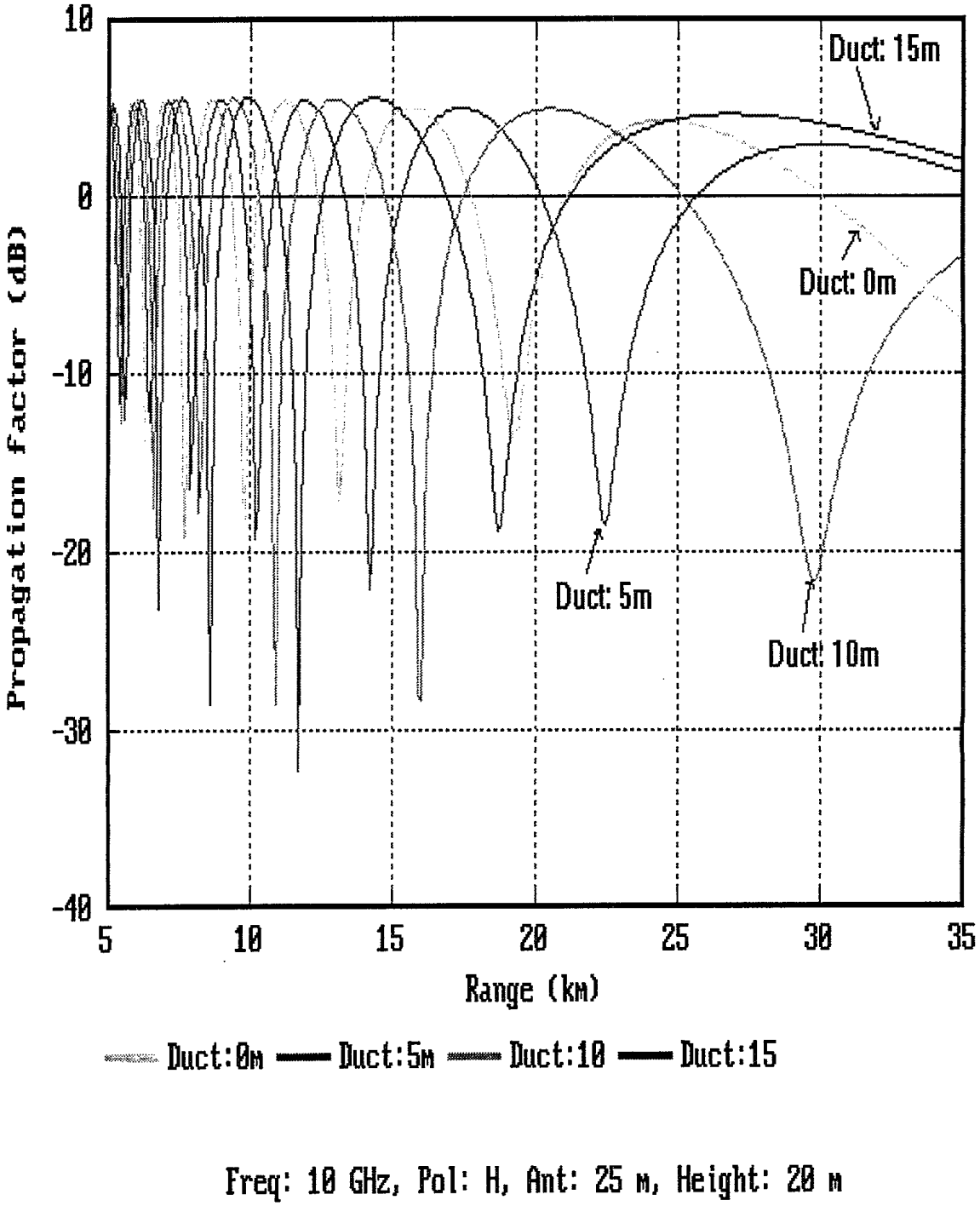

FIGURE 4 - Propagation factor versus range for duct heights of 0,5,10 and 15 m

3.1.3 Antenna Gain Directivity Factor

Radar antennas usually have highly directional properties, with the radiation concentrated in a beam in a particular direction. The effective antenna gain is a function of target azimuth θ and elevation ϕ and is described by a directivity factor, g, of the antenna pattern. Directivity factors are required in the calculation of the propagation factor and the clutter and jamming signals. Using φ as a parameter that can represent either the azimuth θ or the elevation ϕ, four typical directivity factors have been programmed: Isotropic, Gaussian, Sinc(φ), and Cosec.

The first pattern is omnidirectional, the directivity factor is given by

$$g(\varphi) = 1 \qquad [8.]$$

The second pattern is based on the assumption of a Gaussian beam shape; it is normally used to describe a pencil beam

$$g(\varphi) = \exp\left(-4\frac{\varphi^2}{\varphi_b^2}\ln\sqrt{2}\right) \qquad [9.]$$

where φ_b is the half-power beamwidth.

The third pattern is a sinc function; it is used to describe a pencil beam when sidelobes are needed:

$$g(\varphi) = \left(\frac{1+\cos\varphi}{2}\right)\frac{\sin(k\sin\varphi)}{k\sin\varphi} \qquad [10.]$$

with

$$k \cong 1.3916/\sin(\varphi_b/2) \qquad [11.].$$

This pattern can be modified to simulate actual patterns having sidelobe levels considerably lower than 13.26 dB below the main-beam power level by applying a

sidelobe reduction factor. The antenna gain directivity factor is defined inside the main beam by [10] and at angles greater than the first null which occurs at

$$\varphi_{null} = \sin^{-1}(2.2575\sin(\varphi_b / 2)) \qquad [12.]$$

the directivity factor is given by

$$g(\varphi) = 10^{-0.05(S_L - 13.26)}\left(\frac{1+\cos\varphi}{2}\right)\frac{\sin(k\sin\varphi)}{k\sin\varphi} \qquad [13.]$$

where the desired sidelobe level is S_L(dB).

Conventional panoramic surveillance radars are normally described by a cosec-pattern given by

$$g(\varphi) = \frac{\sin(\frac{\varphi_b}{2} + \varphi_{tilt})}{\sqrt{2}}\csc(\varphi) \qquad [14.]$$

The angle φ_{tilt} is the elevation angle of the maximum point of that pattern. A typical value of φ_{tilt} is one-half beamwidth. The directivity factor below the angle (φ_{tilt} + φ_b/2) is represented by a sinc function. Figure 5 gives examples of the four antenna gain directivity patterns actually used in CASE_ATTI sensor module.

3.1.4 Target Cross Section

The mean target cross section σ depends on the target size and shape, the radar wavelength and the target aspect angle. Radar targets such as aircraft, satellites, missiles, and ships can be qualified as point targets when viewed by conventional radars at appropriate ranges. A table can be used to describe σ at a given frequency versus θ' and ϕ' so that the measured σ can be used. Otherwise, the model used to describe the missile-type targets is (Ref. 9) given by:

$$\sigma = \sigma_n \left\{ \left| \cos\left(\sqrt{\phi'^2 + \theta'^2} \right) \right| + \left| \frac{4L}{\pi D} \sin\left(\sqrt{\phi'^2 + \theta'^2} \right) \right| \right\} \qquad [15.]$$

where

σ_n: nose-on cross section (m^2),

ϕ': elevation angle between the line of sight and the target speed vector,

θ': bearing angle between the line of sight and the target speed vector,

L: length of the target (m),

D: diameter of the target (m).

For aircraft and ships at closer ranges, a more sophisticated function of θ' and ϕ' has to be used. A target cross section model for aircraft is given in the SURSEM model (Ref. 4).

3.1.5 Atmospheric Attenuation

Depending on their frequency, electromagnetic waves at RF are more or less affected by oxygen and water vapor. Part of their energy is absorbed and another part is scattered by the encountered particles. The one-way total atmospheric loss (dB) is given by

$$L_{atm} = L_{wo} + R_s(\gamma_{f/c} + \gamma_r + \gamma_{ic}) \qquad [16.]$$

where

L_{wo}: losses due to oxygen and water vapor absorption,

R_S: slant range to the target (km),

$\gamma_{f/c}$: attenuation coefficient (dB/km) caused by fog or clouds,

γ_r: attenuation coefficient (dB/km) caused by rain or snow,

γ_{ic}: attenuation coefficient (dB/km) caused by ice clouds.

The values of various attenuation coefficients as well as the details to calculate L_{wo} are given in Ref. 2.

3.2 System Noise

Natural noise is the ultimate limiting factor in the detectability of radar signals. The origins of this noise lie both within the radar and in the radar environment. The noise power in the receiving system can be expressed in the radar equation in the form of a system noise temperature T_s given by (Ref. 8, p. 152)

$$T_s = T_a + T_t(L_r - 1) + L_r T_0(N_f - 1) \qquad [17.]$$

where

T_t: thermal temperature of the transmission line taken to be 290 K,
L_r: receive loss (taken to be 1/2 $L_{t/r}$),
N_f: receiver noise figure (RF preamplifier, mixer, IF amplifiers),
T_a: noise power received by an antenna from natural external radiating sources, and
T_0 =290 K.

As suggested by Blake, (Ref. 8, p. 172), T_a is given by:

$$T_a = (0.876T_a' - 254)/L_a + 290 \qquad [18.]$$

where T_a' is obtained from Fig. 4.8 of Ref. 8 and L_a is the dissipation loss within the antenna. For reflector antennas and active arrays, the assumption is that $L_a \cong 1$ (Ref. 8, p. 385).

The thermal noise power (watts) at the output of the IF stage is defined as

$$N_0' = kT_s B_N \qquad [19.]$$

where k is the Boltzmann constant (1.38×10^{-23} J/K) and B_N is the noise bandwidth of the receiver in hertz. The actual noise bandwidth varies with the transfer function of the filter or set of filters prior to detection and with the type of waveform. When pulse compression is used, the noise bandwidth is taken as the extended bandwidth of the pulse compression filter ($B_N=1/\tau'$ where τ' is the compressed pulse width).

3.3 Signal-to-Noise Ratio (IF Stage)

The signal-to-noise ratio at the output of the IF stage is given by the ratio of [2] and [19] divided by some additional losses: range-gate loss including average straddling loss (L_g), limiter and quantization loss (L_l) and matching loss (L_m). The S/N_0 is given by

$$\frac{S}{N_0}=\frac{P_r}{N_0'L_x} \qquad [20.]$$

where $L_x = L_g L_l L_m$. In our simulation, we assigned the following typical values for the losses:

L_g (dB) = 2 (Ref. 8, p. 414);

L_l (dB) = 2 (Ref. 10, p. 477), and

L_m(dB) = 1 (Ref. 8, p. 334).

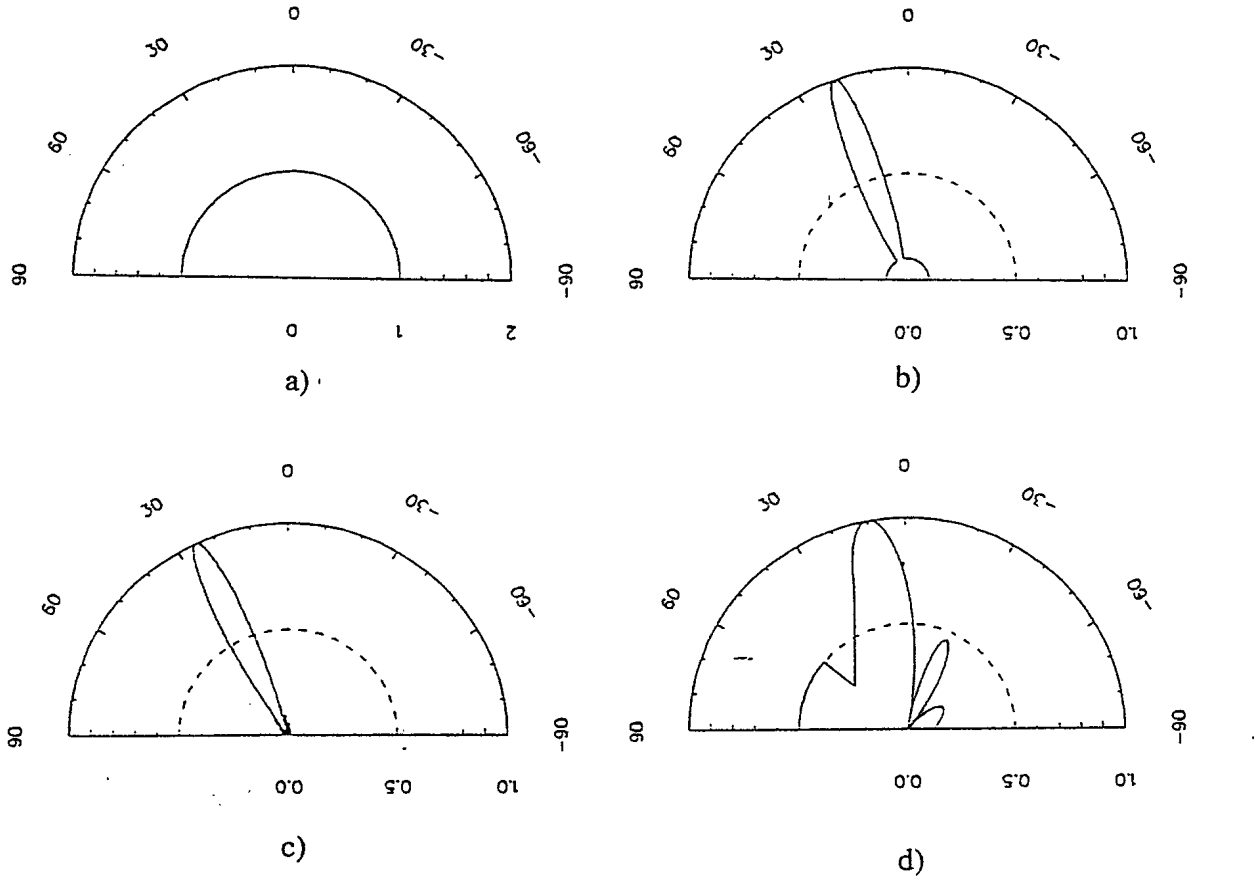

FIGURE 5 - Antenna pattern directivity

a) Omnidirectional
b) Gaussian: (φ_b=10^0, direction 20^0)
c) Sinc: (φ_b=10^0, direction 25^0)
d) Cosec: (φ_b=20^0, direction 10^0)

4.0 INTERFERENCE: CLUTTER AND JAMMING

Clutter and jamming are limiting factors for the detection of targets. In this chapter, the characteristics of these interferences are discussed from the point of view of the radar detection range performance; mean intensity and spectral description are given. This chapter aims at computing the signal-to-clutter and signal-to-jamming ratios at the output of the IF stage just before signal processing takes place at the video stage.

4.1 Clutter

Echoes from the sea and precipitation can produce very significant radar interfering signals. In many cases, these constitute the dominant radar performance limiting factor. As ducting allows radiation to reach targets well beyond the horizon, it similarly makes possible backscattering from beyond the horizon. Because ducting effects on target echoes are important to describe the radar long-range detection capability, ducting must also be considered in the calculation of interference.

The difficulty of calculating the effects of ducting on clutter reflectivity is that these effects have just been recently documented and, although some models have been proposed, no simple model appropriate for our type of radar model has been satisfactorily validated. Nevertheless, we contend that it is preferable to adopt a crude representative model than to simply ignore ducting effects. For sea clutter, we propose an empirical extension based on clutter data reported in the literature, to the widely accepted Georgia Institute Technology (GIT) model (Ref. 11). For precipitation (or weather) clutter, we use the model described in CARPET (Ref. 2) which is appropriate for a surveillance radar.

4.1.1 Sea Clutter Power

In any given range cell, C_R, the mean power received from sea backscattering (at the input of the RF stage) is given by

$$P_{sc} = K_r \frac{g^4(\phi) A \sigma_o^*}{R_{sc}^4} \qquad [21.]$$

where

K_r is the radar constant as defined in [3],

g is the antenna directivity factor in the direction of the illuminated sea patch (unitless),

R_{sc} is the slant range of the illuminated patch (m),

σ_0* is the reflectivity (also known as normalized clutter RCS) of the sea surface per unit area in the cell (m^2 / m^2),

A is the area of the illuminated sea patch (in m^2), which is given by: $A = R_{sc}\theta_b C_R$,

θ_b is the 3-dB horizontal beamwidth (expressed in radians), and

C_R is the range cell (m).

In σ_0*, the asterix means that the reflectivity incorporates ducting effects. Under ducting, large sea backscatter energy can be received from beyond the horizon as energy is reflected against the earth over the horizon. EREPS (Ref. 12) provides a simple means to compute the reflectivity under evaporation ducting but the model is known to significantly underestimate clutter reflectivity under most conditions. Here, the chosen approach is to develop a new empirical model based on published data (Refs. 13-15). The general expression for σ_0* when expressed in dB is

$$\begin{aligned} \sigma_o^*(dB) &= \sigma_o(R_{sc}^*) \quad for \quad R_{sc}^* \le R_{tr} \\ &= \sigma_o(R_{tr}) - 10\beta \log\left[\frac{R_{sc}^*}{R_{tr}}\right] - \Im(R_{sc}^* - R_{tr}) \quad for \quad R_{sc}^* > R_{tr} \end{aligned} \qquad [22.]$$

where

σ_0 is the basic reflectivity as given in textbooks (dB),

R^*_{sc} is the terrestrial range of the clutter patch (km),

R_{tr} is a transition range from where the empirical extension applies (km),

β is the reflectivity decrease coefficient, and

$\Im$ is a clutter propagation loss (dB/km).

For σ_0, the GIT model, as described in (Ref. 11), is used since it is believed by several authors not to be contaminated by refraction effects. The model is valid for frequencies between 1 and 100 GHz. The transition range R_{tc} is taken to be the range at which the grazing angle under ducting begins to differ significantly from the one under standard conditions. Although ray tracing could provide an accurate value of R_{tc}, the use of a rough estimate, applicable for a shipborne-surface sensor, is suggested here for convenience considering the approximate nature of the model extension. When there is no ducting or when ducting can be neglected, (a minimum duct height of 1 m is necessary to declare a ducting condition) R_{tr} corresponds to the horizon range between the antenna and the effective wave height; this is the normal limit of applicability of the GIT model. Mathematically, the transition range can thus be written as

$$\begin{aligned} R_{tr} &= R_H \quad if \quad h_{duct} < 1\,\text{m} \\ R_{tr} &= R_{tc} \quad if \quad h_{duct} \geq 1\,\text{m} \end{aligned} \qquad [23.]$$

with

$$R_H = 3.57\left(\sqrt{h_a} + \sqrt{h_e}\right) \qquad [24.]$$

and

$$R_{tc} = 7.1 - 3.6 \log h_{duct} \qquad [25.]$$

where

h_a: antenna height (m);

$h_e = 0.375 w_h$, where w_h is the *significant* wave height (see Ref. 10, p. 273);

h_{duct}: duct height (m).

Data published in the literature indicate that β can vary from 4 to about 1 when the conditions go from standard to optimal ducting conditions. The optimal duct height (i.e. for which surface energy is maximum) depends on the radiated frequency. It can roughly be estimated by

$$h_{duct(opt)} = 37 - 8.69 \ln(f) \qquad [26.]$$

where f is the frequency in GHz. Simple linear relationships are used to estimate β for low sea state, S_{sea} (sea state 2 and below), based on the data found in the literature. For higher sea states, a correction is applied. Consequently, β can be expressed as

$$\begin{aligned} \beta &= \beta^{\circ} \quad if \quad S_{sea} < 2 \\ \beta &= \beta^{\circ}\left[\frac{(S_{sea}-2)}{4}+1\right] \quad if \quad S_{sea} \geq 2 \end{aligned} \qquad [27.]$$

with

$$\begin{aligned} \beta^{\circ} &= 4 - \frac{3}{h_{duct(opt)}} h_{duct} \quad if \quad h_{duct} \leq h_{duct(opt)} \\ \beta^{\circ} &= 1 + \frac{3}{30 - h_{duct(opt)}} (h_{duct} - h_{duct(opt)}) \quad if \quad h_{duct} > h_{duct(opt)} \end{aligned} \qquad [28.]$$

For frequencies less than 10 GHz, reported data show a slightly greater decrease in reflectivity with range than that given by the second term of equation [27]. A clutter propagation loss, $\Im$, has then been incorporated to match the published data better. When ducting is negligible or absent, $\Im$ is used to describe the steep decrease of reflectivity beyond the horizon. The parameter $\Im$ is given by

$$\Im = 3.6 \quad \text{for} \quad h_{duct} < 1\,\text{m}$$
$$\Im = \frac{\beta+1}{4}\log[-0.9(f)+9] \quad \text{for} \quad h_{duct} \geq 1\,\text{m} \quad \text{and} \, f < 10\,\text{GHz} \qquad [29.]$$
$$\Im = 0 \quad \text{for} \quad h_{duct} \geq 1\,\text{m} \quad \text{and} \, f \geq 10\,\text{GHz}$$

Figure 6 shows σ_0^* versus range with and without ducting for a frequency of 9.8 GHz using vertical polarization. The antenna height is 25 m and the duct height is 10 m. Wind speed and wave height are 4.5 m/s and 1 m, respectively.

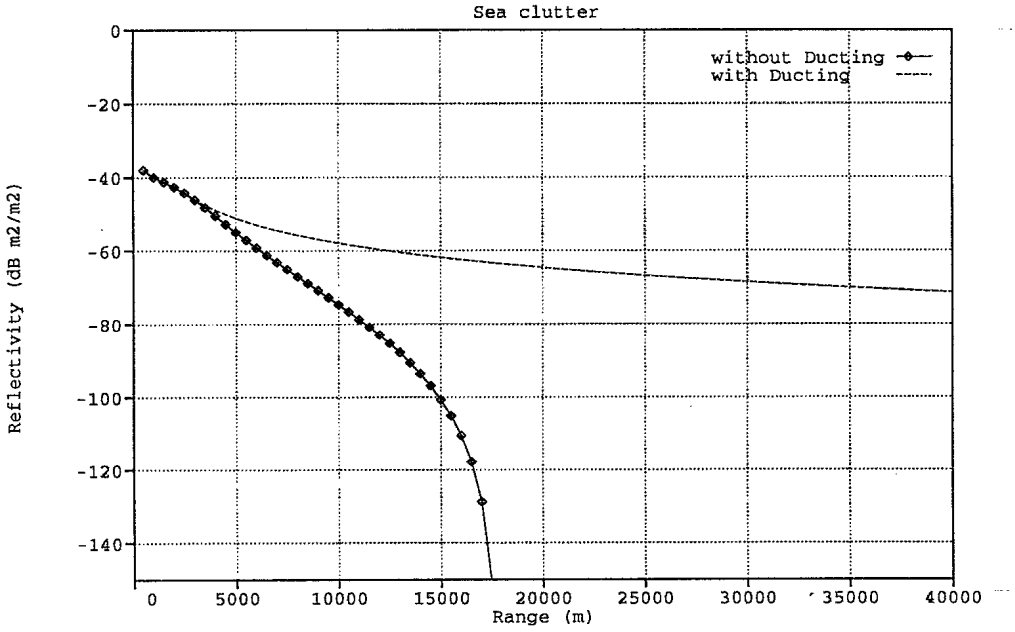

FIGURE 6 - Ducting effects on sea-clutter reflectivity

4.1.2 Sea-Clutter Power Distribution Skewness

The models developed for the generation of the clutter false alarms (see Section 7.2) and for the estimation of the clutter distribution loss (L_d) in the clutter filtering process (see Section 5.2) require estimates of the skewness of the clutter power distribution with respect to Rayleigh. For medium-to-high resolution radars, distributions

of clutter return have a longer tail than Rayleigh distributions for large-amplitude clutters; the median can differ significantly from the mean value. Unfortunately, the literature on the subject is insufficient to safely establish the relationship between clutter distribution and the depending radar and environmental parameters. However, representative guesses can be made based on measurements recently published.

Let us define the product beamwidth-pulselength, $X = \theta_b \tau'$ (in degree-μs), to describe radar resolution. According to the published data (Ref. 10, Fig. 7.14 and Refs. 16-17), non-Rayleigh distributions are obtained for $X < 4$ ^{o}-μs when the pulselength is shorter than 4 μs. For greater X and pulselength values, Rayleigh distributions are assumed.

To characterize non-Rayleigh distributions, the Weibull formulation is used. Weibull distributions, which are described with only a few parameters (which can be related to the physical conditions of operation), have proven to be, in general, better than log-normal distributions to describe the statistical behavior of clutter signals. With Weibull, the mean and median reflectivity are adapted from Ref. 18 as:

$$\sigma_0^{50} = \sigma_0 - 1.6a - 10\log(\Gamma(1+a)) \qquad [30.]$$

where σ_0^{50}, the median reflectivity, and σ_0, the mean reflectivity, are both expressed in dB, Γ is the gamma function and a is the unitless Weibull parameter. As detailed in Chapter 7, the parameter a characterizing the Weibull distribution can be used in conjunction with the calculated mean reflectivity (previous section) to estimate the distribution of clutter false alarms. In addition, the median-mean difference is used to estimate the degradation of the *S/I* improvement of the clutter filtering process (called distribution loss) (see Section 5.2). The parameter a depends on the radar characteristics (e.g. resolution, frequency, polarization) and the environmental conditions (wind and grazing angle). For medium-to-high-resolution radars, as defined above, values of a are

estimated in the radar domain (R,θ) and stored in the clutter map file together with the calculated reflectivities.

From experimental results, Ref. 19 shows that a varies roughly linearly with the logarithm of wind speed. For our model we use

$$a_{ref} = \max(a_{\min}, 3\log w_s) \qquad [31.]$$

where w_s is the wind speed in m/s. This relationship is valid at X-band (9.8 GHz), upwind conditions and at 3° grazing angle. To obtain the a value in any conditions, we use a relationship between a and the magnitude of the mean backscatter. Reference 19 shows that a varies linearly with the magnitude of the mean backscatter when expressed in dB. Consequently, the effective a parameter can be given by:

$$a = \max(a_{\min}, 0.066\sigma_{0d} - a_{ref}) \qquad [32.]$$

where σ_{0d} is the difference in dB between the evaluated mean reflectivity σ_0 for the conditions under study and the σ_0 under the referenced condition stated above. The difference σ_{0d} must then be precomputed in addition to σ_0^* and stored in the clutter table.

For increasing range (or decreasing grazing angle) the resolution cell widens, which could logically contribute toward Rayleigh distribution. Reference 20 shows how a is likely to decrease with increasing resolution cell volume. This further correction of a was not adopted as some tests made using various measurements found in the literature showed that in most cases the resulting a's are within the margin of uncertainty of [31] and [32]. In our model, the decrease of a versus range is then essentially governed by the decrease of σ_0 with range (i.e. with decreasing grazing angle).

Some authors suggest that a can get smaller than 1 when the distribution tends to Rayleigh. As explained in Chapter 7, for the generation of clutter-induced false alarms, it is convenient to have this number adjustable by the user. While a small variation of a_{min}

can affect false alarm density, it has no significant impact on the clutter filtering distribution loss.

The method described above for estimating the skewness of the sea-clutter distribution is based on clutter statistics which apply for vertical polarization (VP) exclusively, as they essentially describe the Bragg scatter component of clutter (Ref. 21). Unfortunately, the very few clutter data published so far in the literature for horizontal polarization (HP) prevent us from deriving a similar model for HP radar emissions. Although mean backscatters are weaker in HP, in general, distributions have longer tails for the same conditions. Furthermore, the median-to-mean difference, a skewness indicator, has often been found to be maximum at sea state 2 and to decrease very slightly from sea state 2 to sea state 5. Consequently, in the simulation, until more information is found in the literature, for horizontal polarization, we propose to use a high value of a, $a_{\max}^{HP}$, , at close range (reference range corresponding to a grazing angle of 3^{o}) for any wind speeds and to perform a smooth linear decrease of a so that a reaches a_{min} at the range where the received clutter power gets down to $2N_0'$ (i.e. twice the thermal noise power (see [19]); $a_{\max}^{HP}$ is arbitrarily taken to be 3.0, which corresponds to a relatively adverse condition.

4.1.3 Sea-Clutter Spectrum

The sea-clutter spectrum width and shape are the results of the spread of velocities of the elemental scatterers of the sea surface. The width of this spectrum is an important factor in assessing the performance of clutter rejection techniques. A Gaussian spectrum shape with a standard deviation σ_s yields

$$P_c(f) = P_{sc} \exp\left\{-\frac{1}{2}\left(\frac{f-\mu_c}{\sigma_s}\right)^2\right\} \qquad [33.]$$

The mean μ_c is a function of relative motion between the radar platform and the clutter. The standard deviation of the clutter spectrum is a measure of the bandwidth of the clutter spectrum. The spectral distribution of the clutter is a function of various factors such as platform motion, internal clutter motion, system instabilities and transmitter drifts.

The radar platform motion creates two effects. The first is the shifting of the center frequency of the clutter spectrum as a function of the antenna pointing direction relative to the platform motion. The second is the broadening of the clutter spectrum resulting from platform motion normal to the antenna pointing direction. The finite beamwidth of the antenna illuminates an area on the ground or sea, which contents components having a different Doppler velocity with respect to the radar. The Doppler frequency corresponding to the closing velocity between the antenna and the center of the clutter patch is given by

$$f_1 = 2\left(\frac{v_s}{\lambda}\right)\cos\theta_a \sin\psi_d \qquad [34.]$$

where

v_s is the ship velocity (m/s),

θ_a is the azimuth angle between the platform velocity vector and the direction of the antenna beam,

Ψ_d is the depression angle for a shipborne antenna.

There can also be a Doppler shift due to the average radial velocity of the waves relative to the radar, which is typically a few knots (0.5 m/s). The mean Doppler shift μ_c is

$$\mu_c = f_1 - k_{vw} \qquad [35.]$$

where k_{vw} is roughly $1/\lambda$. Some radars compensate for the platform motion and in this case μ_c=0.

The width of the clutter spectrum is the sum of several components: wind shear, finite antenna beamwidth, radar system instabilities, etc. The scatterers forming the clutter return often move in the wind causing a frequency spreading of (Ref. 10)

$$\sigma_1 = \frac{w_s \cos\phi_w}{2\lambda} \qquad [36.]$$

where σ_1 is expressed in Hz and

w_s is the wind speed (m/s), and

ϕ_w is the direction of the wind (with respect to true-north).

If the radar antenna is rotating, an additional σ_r resulting from the antenna rotation has to be considered, where (Ref. 10, eq. 9.76)

$$\sigma_r = \frac{\alpha}{5.35\theta_b} \qquad [37.]$$

where α is the antenna rotation rate in rd/s and θ_b is the azimuth beamwidth (in rd).

Then, the resultant standard deviation of the sea-clutter spectrum is given by

$$\sigma_s = \sqrt{\sigma_1^2 + \sigma_r^2}. \qquad [38.]$$

4.1.4 Weather-Clutter Power

Raindrops and other forms of precipitation are significant reflectors of radar waves and thereby can produce an appreciable clutter echoes. The power received from such echoes at the input of the receiver is given by

$$P_{wc} = K_r \frac{\vartheta}{R_{wc}^4} \qquad [39.]$$

where K_r is as previously defined, R_{wc} is the slant range of the target (m) and ϑ represents the cross section of the volume cell.

For a surveillance radar where the beam is at the horizon, the model described in CARPET (Ref. 2) is adequate. The cross section, ϑ, is given by

$$\vartheta = \vartheta_0 R_c \theta_b d_h C_R \qquad [40.]$$

with

$$R_c = \mathrm{mod}(R_t, \tfrac{c}{2f_r}) \qquad [41.]$$

and where:

ϑ_0 is the weather reflectivity (m^2/m^3),
R_t is the terrestrial distance between the target and the antenna (m),
C_R is the range gate (m) (= $c\tau'/2$, where c is the speed of light and τ' is the compressed pulsewidth),
d_h is the height of the volume cell.

The weather reflectivity ϑ_0 is a function of the precipitation rate, p_r (mm/h), and the frequency, f (GHz). It is computed using the general expression:

$$\vartheta_o = K f^4 p_r^{1.6} \qquad [42.]$$

where
$K = 7 \times 10^{-48}$ when $f \le 6$ GHz
$K = 13 \times 10^{-48}$ when $f \ge 35$ GHz

For 6 GHz $< f <$ 35 GHz, K is obtained from a linear interpolation between 7 x 10^{-48} and 13 x 10^{-48}. This formula is valid for rain-type precipitation. Snow precipitation rate must then be converted in rain equivalent precipitation rate. For dry snow, the rain equivalent

rate is accepted to be 10 times less than the actual snow precipitation rate, while for wet or melted snow the ratio is expected to be less. A ratio of 5 is suggested in the latter case.

The height of the cell volume is given by:

$$d_h = \min(h_{cloud}, R_c \phi_b) \qquad [43.]$$

where h_{cloud} is the height of the cloud base (height of the rain volume) and ϕ_b is the elevation beamwidth.

4.1.5 Weather-Clutter Spectrum

The relative motion of the reflectors produces a spread of velocities and consequently a spread of Doppler frequencies. A Gaussian assumption is used to approximate the weather clutter-spectrum shape. Its standard deviation (in Hz) is determined by (Ref. 10)

$$\sigma_{wc} = \frac{2}{\lambda}\sqrt{\sigma_{shear}^2 + \sigma_{turb}^2} \qquad [44.]$$

with

$$\sigma_{shear} = 0.42 \times 4 \times 10^{-3} R \theta_b \qquad [45.]$$

where

σ_{shear} is the wind shear standard deviation (Hz)
σ_{turb} is the standard deviation of the turbulence (Hz)

An additional deviation due to antenna rotation is added as in the case of clutter sea spectrum.

4.1.6 Signal-to-Clutter Ratio

The signal-to-sea-clutter and the signal-to-weather-clutter ratios at the output of the IF stage are given by the ratio of P_r/P_{sc} and P_r/P_{wc} both affected by the receiver losses, L_c:

$$\frac{S}{C} = \frac{P_r}{(P_{sc} + P_{wc})L_c} \qquad [46.]$$

where $L_c(\text{dB}) = L_x + 1$ dB, i.e. 1 dB more than the loss, L_x, used when only system noise is present, as slightly greater losses are expected in the presence of clutter (Refs. 8 and 10).

4.2 Jamming

Only standoff noise sidelobe radar jamming is considered in this model. In standoff jamming, the jammer stands off from the radar at a fixed position. This noise jamming has the same effect on the target detection as does natural noise; the only essential difference being its magnitude.

The power of the jamming, P_j is given by

$$P_j = \frac{P_{jt} G_r G_j L_{sl} B \lambda^2 F_j^2}{(4\pi)^2 R_j^2 L_r L_{atm} B_j} \qquad [47.]$$

where

P_{jt}: transmitted jammer power

G_r: radar receiving antenna gain

G_j: jammer antenna gain

L_{sl}: azimuth sidelobe radar antenna level with respect to main beam

B: radar beamwidth

F_j: one-way propagation factor

R_j: jammer range

L_r: receive loss

L_{atm}: one-way atmospheric losses

B_j: jammer bandwidth

4.2.1 Signal-to-Jamming Ratio

The signal-to-jamming ratio at the output of the IF stage is given by the ratio of P_r/P_j affected by receiver losses such as

$$\frac{S}{J} = \frac{P_r}{P_j}\frac{1}{L_j} \qquad [48.]$$

where $L_j = L_x$ as in the case of system noise.

5.0 RADAR SIGNAL PROCESSING

The performance of the radar detection process depends on the signal processing capability to reject the undesired interference. The objective of this chapter is to compute the *S/I* ratio at the output of the video stage where signal processing is applied. The signal processing yields enhanced signal power relative to clutter and noise power. This enhancement is termed an improvement factor.

5.1 Improvement Factor Calculation

Velocity filtering for modern radar systems have been made mainly through moving target indicators (MTI) and with pulse Doppler radars. MTI is normally used with low-pulse-repetition-frequency (low-PRF) radars. The MTI is usually a single filter that rejects clutter by means of a notch in its passband centered on the clutter Doppler spectrum. Pulse Doppler is usually associated with high-PRF radars. A contiguous bank of narrow-band filters is used to detect moving targets outside of the clutter spectrum. This section presents the improvement factor of M-pulse MTI cancelers as well as the improvement factor obtained with a coherent integrator (bank of narrow filters).

Both the MTI and the coherent integrator can be modeled as a transversal filter where the output $y(t)$ consists of a weighted sum of the input $x(t)$ such as

$$y(t) = \sum_n w_n x(t - nT) \qquad [49.]$$

where T is the time between samples, n is the filter tap number and while the weights w_n may be complex.

The transversal filter described by [49] depicts only one filter and one output. However, multiple independent outputs are possible by selecting appropriate weights. In, particular, the FFT weights form n filters with n outputs. The signal gain of a particular filter is found, provided that the Doppler frequency, f_d, is such that a signal exists

somewhere between the crossover points of adjacent filters. The gain of the i^{th} filter is derived by considering a target Doppler f_d that can occur with equal probability in the region

$$f_i - B/2 \le f_d \le f_i + B/2 \qquad [50.]$$

where f_i is the center of the response of the i^{th} filter and B the filter bandwidth.

The probability density function for f_d associated with the i^{th} filter is

$$P(f_d) = \frac{1}{B} \quad \text{for} \quad f_i - B/2 \le f_d \le f_i + B/2$$
$$= 0 \quad \text{elsewhere} \qquad [51.]$$

The received signal waveform can be represented by

$$r(t) = s(t)\exp(j2\pi f_d t) \qquad [52.]$$

where $s(t)$ takes into account target's characteristics, transmitted waveform, radar stability antenna scanning and so on, and f_d is the Doppler frequency corresponding to the relative velocity between radar and target. If the Doppler shift is the dominant effect then the autocorrelation of eq.[52] is

$$\psi(\tau) = \exp(j2\pi f_d \tau) \qquad [53.]$$

The expected value of ψ is

$$E\{\psi(\tau)\} = \int_{-\infty}^{\infty} \exp(j2\pi f_d \tau) P(f_d) df_d = \exp(j2\pi f_i \tau)\frac{\sin(\pi B\tau)}{\pi B\tau} \qquad [54.]$$

and, consequently, the signal covariance matrix $\mathbf{M}_s$ becomes

$$\mathbf{M}_s(k,l) = \exp\left(-j2\pi(f_i/f_r)(k-l)\right)\frac{\sin(\pi(B/f_r)(k-l))}{\pi(B/f_r)(k-l)} \qquad [55.]$$

It is convenient to assume a Gaussian clutter spectrum. When the clutter spectrum departs from the Gaussian assumption, a distribution loss is taken into account in the overall processing gain computation (next section). Assuming stationarity, the $(k,l)^{th}$ element of the clutter covariance matrix, $\mathbf{M}_c$, is obtained by taking the Fourier transform of [55], which results in

$$\mathbf{M}_c(k,l) = \exp\left(-2(\pi\sigma_s/f_r)^2(k-l)^2 - j2\pi(\mu_c/f_r)(k-l)\right) \qquad [56.]$$

The improvement factor, I_F, of any arbitrary transversal filter specified by a weight vector $\mathbf{w}$ can be computed using

$$I_F = \frac{\mathbf{w}^H\mathbf{M}_s\mathbf{w}}{\mathbf{w}^H\mathbf{M}_c\mathbf{w}} \qquad [57.]$$

where $\mathbf{w}^H$ is the transposed complex conjugated of the weight vector associated with the filter of interest.

5.1.1 MTI Filters

The improvement factor of an n-stage MTI can be computed by using [57]. The matrix $\mathbf{M}_s$ is generated using [55] and by letting $f_i = 0.5f_r$, i.e.the center of the filter is at one-half the pulse repetition frequency. The covariance matrix, $\mathbf{M}_c$, is generated using [56], with the average Doppler clutter μ_c brought back to zero. The column vector $\mathbf{w}$ can be given by the binominal coefficients with alternating signs, i.e.

$$w_i = (-1)^{i-1}\binom{n}{i-1} \qquad \text{for } i = 1,2,\ldots,n+1 \qquad [58.]$$

5.1.2 Bank Of Narrow Band Filters

Here we consider the more general approach of passing the data through a bank of narrow-band filters. Since the noise is wideband, its energy is divided among various filters. However, each target return has its energy concentrated at one specific Doppler frequency. A bank of narrow-band filters actually reduces the average value of the noise by eliminating many of its frequency components. We consider here two classes of Doppler filter bank, the weighted Discrete Fourier Transform (DFT) and Finite Impulse Response (FIR) filter banks.

The DFT filter bank comprises a set of filters that have identical characteristics, except for the mainlobe position. Identical filters can be synthetized using the FFT (Fast Fourier Transform). FFT filters represent a restricted class of FIR filters having weighting coefficients that are not optimum because they cannot be defined independently for each filter. The FIR technique is more flexible than the DFT technique for the design of the filter transfer function. This is because its weights can be changed for different environments thus changing the sidelobe characteristics of the filter. If necessary, the FIR technique allows for filters that are non-identical in order to concentrate the low sidelobes in the frequency range of the clutter interference.

The improvement factor for coherent integration (bank of filters) is computed the same way as for the MTI filters. Equation 57 is used with the weight vector **w** generated using

$$w_{kn} = \exp\left(-j2\pi\frac{(n-1)(k-1)}{N}\right) \quad \text{for } n = 1,2,\ldots,N. \qquad [59.]$$

where k is the filter index and N the number of filters. The signal covariance matrix $\mathbf{M}_s$ is generated using [55], with the bandwidth B given by $1/N$. The center of the i^{th} filter, f_i, is given by

$$f_i = \frac{i-1}{N} \quad \text{for} \quad i = 1,2,\ldots,N \qquad [60.]$$

5.1.3 Cascaded MTI and Coherent Integrator

In this case, the improvement factor is calculated still using [57]. The MTI filter is characterized by the number M of pulses processed and by a weight vector **a**. The coherent integrator is characterized by the number N of pulses it processes and by its weight vector **b**. The number M is always less than N. The cascaded combination of filters can be evaluated as outlined for the MTI filters or for the bank of narrow-band filters. The only difference is that the weight vector **w** is generated the following way:

$$\mathbf{w} = \begin{bmatrix} a_1 & 0 & 0 & \cdots & 0 \\ a_2 & a_1 & 0 & \cdots & 0 \\ \vdots & a_2 & a_1 & \cdots & \vdots \\ a_M & \vdots & a_2 & \ddots & 0 \\ 0 & a_M & \vdots & \ddots & a_1 \\ 0 & 0 & a_M & \ddots & a_2 \\ \vdots & \vdots & \vdots & \ddots & \vdots \\ 0 & 0 & 0 & \cdots & a_M \end{bmatrix}_{M\times(N-1)} \begin{bmatrix} b_1 \\ b_2 \\ b_3 \\ \vdots \\ b_{N-1} \end{bmatrix}_{(N-1)} \qquad [61.]$$

5.1.4 Improvement Factor with Staggered PRF

We use here the results of Ref. 22 where the effects of staggered PRF on the MTI improvement factor performance is investigated. They conjecture that the minimum clutter output of a staggered PRF MTI system is bounded by the performance of two equivalent constant PRF MTI systems. One of them has a PRF equal to the lowest PRF of the staggered PRF system, while the other has a PRF equal to the highest PRF of the staggered system. In our computation we take the average of both.

5.1.5 Data Windowing

The sidelobe levels of the Doppler filters can be reduced by using a data window function. This corresponds to weighting the input time samples $x(n)$ by a weight vector $a(n)$ such as

$$w(n) = a(n)x(n) \qquad [62.]$$

where $a(n)$ can be chosen from a variety of window functions (Ref. 23) for a desired filter shape. The improvement factor is then calculated using [57].

5.2 Clutter Distribution Loss

In modern radars, short pulselengths (high resolution) are often priviledged in order to minimize clutter returns as the returned mean power is directly proportional to the resolution cell size. However, as a drawback, sea-clutter spectrum widen and the amplitude distribution shows longer tail (for strong returns) with increasing resolution, which makes sea clutter more difficult to filter out.

For medium-to-high resolution radars, a loss, called clutter distribution loss, is heuristically estimated to account for the degradation of the improvement factor, I_F, in non-Rayleigh clutter when sea clutter is found to be the dominant clutter source. The conditions for identifying medium-to-high resolution radars are as defined in Subsection 4.1.2. In our model, we assume that the losses presented by Schleher (Ref. 24), as a function of I_F and the clutter mean-to-median ratio, describe the radar filtering efficiency degradation.

From Fig. 1 of Ref. 24, we come up with the approximate expression for the clutter distribution loss L_d:

$$\begin{aligned} L_d &= L_{d0} \qquad for \qquad 0 < I_F < 20 \text{ dB} \\ &= L_{d0} \exp\left(-(I_F - 20)^2 / 100\right) \qquad for \qquad I_F \geq 20 \text{ dB} \end{aligned} \qquad [63.]$$

This relationship is believed to provide realistic values of L_d for P_d vaying from 0.5 to 0.8, the normal threshold of detection. L_{d0} can be approximated by:

$$L_{d0} = 15\left(1 - \exp\left(-d_{mm}/8.45\right)\right) - 5 \qquad [64.]$$

where d_{mm} is the difference between the median and the mean clutter return. For any given radar cell, d_{mm} can be calculated from [30] (Subsection 4.1.2) using the Weibull parameter a and the mean clutter reflectivity given in the clutter map table.

5.3 Processing Gain

The processing gain, G_p, of the video stage is consequently given by

$$G_p = \frac{I_F}{L_d}. \qquad [65.]$$

An example of computation of I_F is given in Fig. 7 where five FIR filters with 32 Hanning filter taps have been used. The I_F is plotted versus Doppler frequency normalized with respect to PRF. The oscillations on the curve are caused by a phenomenon called the scalloping or picket-fence effect. The scalloping effect is the observed dip in the improvement factor for a Doppler frequency lying midway between two filters.

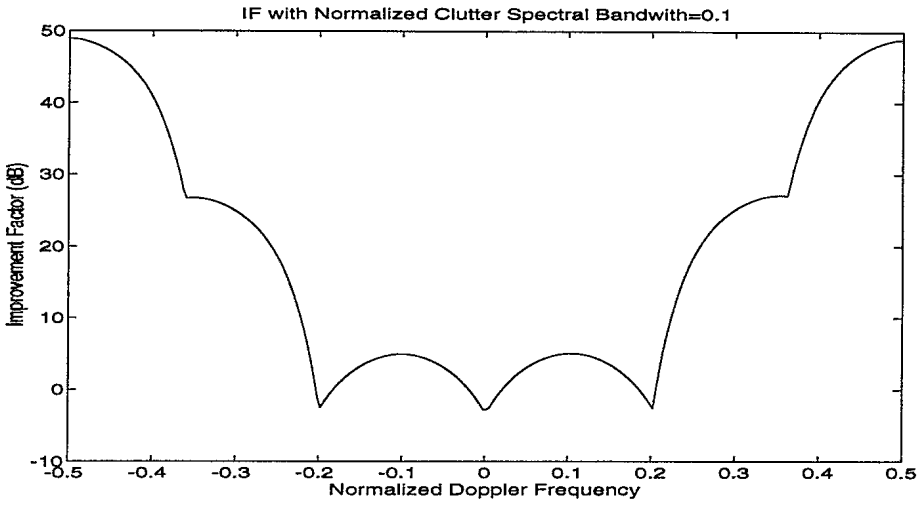

FIGURE 7 - Improvement factor versus normalized Doppler frequency for a bank of 5 FIR filters

6.0 TARGET CONTACTS

A target is detected when the received signal exceeds a pre-set threshold which depends on a desired probability of false alarm P_{fa}. The probability that the threshold be exceeded due to the presence of a target, i.e. P_d, depends on noise, clutter and jammer statistics, threshold level and integration of pulses as the beam sweeps the target. In the previous chapters, we calculated the necessary components to evaluate the signal-to-interference energy ratio resulting from the reception and processing. In this chapter, the *S/I* ratio is used to calculate the probability of detection for a given false-alarm probability. Then, "realistic" target contacts measurements are generated according to P_d and the accuracy of the sensors.

6.1 Calculation of the Signal-to-Interference Ratio

The equivalent *S/I* ratio per pulse is calculated according to the following expressions. When thermal noise is dominant (i.e. $N_0' > 2C > J$ where C results from both sea and weather clutter), *S/I* is given by

$$\frac{S}{I} = \frac{S}{N_0} G_p \frac{1}{L_{CFAR}} \qquad [66.]$$

where L_{CFAR} is the loss associated to set up the threshold. When thermal noise is dominant, L_d=1. In CFAR system, the threshold is constinuously adjusted at some factor times the noise estimated from a second reference channel. When the number of samples of noise in the reference channel is reduced, the sampled reference noise will fluctuate appreciably and a higher threshold must be set up. L_{CFAR} corresponds to a loss in signal detectability. A value of 1.5 dB, which is a likely average value for operational systems (Ref. 8), has been assigned to L_{CFAR}.

When the clutter is dominant (i.e. $C \geq N_0'/2$), the *S/I* is given by

$$\frac{S}{I} = \frac{S}{C} G_p \frac{1}{L_{CFAR} L_{cd}} L_B \qquad [67.]$$

where L_{cd} describes a decrease in detection sensibility when the clutter amplitude distribution is non-Rayleigh. A value of 2 dB has been assigned to L_{cd}, which correspond to a likely trade-off for theshold setting in order to optimize detectability while maximazing clutter rejection (Ref. 18). For the beam shape loss L_B , the conventional value of 1.6 dB from Blake (Ref. 8) is applied.

When jammer is dominant ($J > 2(C+ N_0')$), it is similar to thermal noise.

6.2 Calculation of the Probability of False Alarms

In radar specifications, the mean time between false alarms, $t_{fa,}$ is the parameter that describes the desired false alarm rate instead of the probability of false alarm, which is used in the calculation of the probability of detection. As discussed in Ref. 10, the probability of false alarm P_{fa} is given by:

$$P_{fa} = \frac{0.69}{n'} \qquad [68.]$$

where n' is the number of independent opportunities for a false alarm in the mean time between false alarms, t_{fa}. Defining n_0 as the number of opportunities during the beam sweep period over any potential point target, and t_{swp} the processing time required to determining whether or not a target is present, n' can be expressed as:

$$n' = n_0 \, t_{fa} / t_{swp} \qquad [69.]$$

where

$$t_{swp} = \frac{\theta_b}{2\pi} t_{scan} \qquad [70.]$$

and

$$n_0 = N_{ch} N_{rc} \qquad [71.]$$

where

t_{scan} is the time of one radar revolution (s),

θ_b is the horizontal 3 dB beamwidth (rad),

N_{ch} is the number of radar decision channels (unitless integer), and

N_{rc} is the number of range cells.

The number of range cells is given by

$$N_{rc} = \frac{1}{f_r \tau'} - 2 \qquad [72.]$$

where f_r is the pulse repetition frequency (Hz) and τ' is the compressed pulse length (s). In our model, the number of decision channels per cell, N_{ch} is taken to be 2 for any radar.

6.3 Effective Number of Pulses Available for Noncoherent Integration

When system noise or jamming are the dominant sources of interference, we assume that the interfering signal is Gaussian and uncorrelated. We also assume that, in this case, clutter filtering stages are switched off by the operator. Consequently, the number of pulses available for non-coherent integration is the number of pulses that hit the point target during a beam sweep, which is given by

$$N_n = t_{swp} \cdot f_r \qquad [73.]$$

When clutters dominate as sources of interference, the interfering signals are correlated; this contributes to decrease the effectiveness of the non-coherent integration of pulses. To account for the integrator performance degradation, we define an effective number of pulses available for the integration, N_e , which is a number between 1 and N_n depending on the radar and clutter characteristics. As explained by Nathanson (Ref. 10

pp. 89-92), the nominal effective number of pulses, here defined as N_n', can be understood as the number of independent (or uncorrelated) pulses; it can be approximated by

$$\begin{aligned} N_n' &= [N_n] \quad if \quad (\sigma_s'/\lambda f_r) \geq 0.2 \\ N_n' &= [1 + 5\sigma_s'\theta_b/6\lambda f_{rot}], \quad else. \end{aligned} \qquad [74.]$$

where λ is the wavelength (m) and σ_s' is the standard deviation of the clutter velocity spectrum (m/sec).

In most modern radars, the sampling rate is such that clutter samples are highly correlated and thence N_n' is very small (i.e. 1 or 2) under most conditions. However, frequency agility, which is often employed, is a means to decorrelate clutter samples. Therefore, the effective number of pulses available for non-coherent integration before (or without) MTI processing, hereafter referred to as N_e', can be generalized by the expression:

$$N_e' = \max\left(N_n/N_{fc}, N_n'\right) \qquad [75.]$$

where N_{fc} is the number of pulses before a frequency change (as given in the radar specifications).

MTI filtering contributes to further correlate incoming interfering signal and thus to decrease the number of effective pulses. Assuming that the N_e' pulses as obtained above are as uncorrelated as system noise (so that they can be considered like noise pulses), the number of effective pulses at the ouput of the MTI filtering can be approximated using a fit on theoritical results published by Trunk (Ref. 25):

$$N_e = \frac{N_e'}{1 + 0.53N_{pc}} \qquad [76.]$$

where N_{pc} is the order of the MTI filter (N_{pc}-pulse canceler).

Finally, when filter bank or coherent integration is used instead of MTI the effective number of pulses available for post-integration is (Refs. 8, 10):

$$N_e = N_n / N_c \qquad [77.]$$

where N_c is the number of pulse coherently integrated.

6.4 Calculation of the Probability of Detection

A convenient and conceptually simple approach based on the widely accepted Blake procedure (Ref. 8) is used to calculate the probability of detection. In Blake's approach, a minimum signal-to-noise ratio is determined to achieve a given probability of detection and false alarm. Our approach differs in that the probability of detection is determined from an equivalent (*S/I*) ratio per pulse.

A fairly general approximation of the equivalent *S/I* per pulse, D_0, for the detectability of steady state targets is

$$D_0(N_e) = \frac{X_0}{4H_n}\left(1+\sqrt{1+\frac{16H_n}{\zeta X_0}}\right) \qquad [78.]$$

where

$$X_0 = \left(g_{fa} + g_d\right)^2 \qquad [79.]$$

$$g_{fa} = 2.36\sqrt{-\log P_{fa}} - 1.02 \qquad [80.]$$

$$g_d = \frac{1.231t}{\sqrt{1-t^2}} \qquad [81.]$$

$$t = 0.9(2P_d - 1) \qquad [82.]$$

with

H_n: equivalent number of pulses integrated,

ζ: asymptotic efficiency of the envelope detector,

N_e: number of integrated pulses (calculated in the previous section).

This formula is valid over the range $0.1 \leq P_d \leq 0.9$ and for $10^{-12} \leq P_{fa} \leq 10^{-4}$ with a maximum error of 0.7 dB when compared with theoretical curves (Figs. 2.4-2.8 of Ref. 8). The equivalent number of pulses integrated, H_n, for several types of integrator and two signal variation models is given in Table I (Ref. 8, p. 68).

TABLE I

Equivalent number of pulses integrated for different kind of integrators

SIGNAL VARIATION	INTEGRATOR	H_n
Gaussian	Non-uniform weight	$0.626\ N_e$
Gaussian	Uniform weight	$0.558\ N_e$
Gaussian	Single-loop feedback	$0.561\ N_e$
Gaussian	Double-loop feedback	$0.586\ N_e$
Constant	Non-uniform weight	N_e
Constant	Uniform weight	N_e
Constant	Single-loop feedback	$1.4299\ N_e$
Constant	Double-loop feedback	$1.3347\ N_e \exp(-3/N_e)$

Table II gives the asymptotic efficiency ζ for the three envelope detectors.

TABLE II

The asymptotic efficiency of three envelope detectors

ENVELOPE DETECTORS	ζ
Square law	1.0
Linear law	0.915
Logarithmic law	0.608

The probability of detection P_d is obtained by an iterative procedure to an accuracy of 1% of the input *S/I* ratio. Equation 78 is valid for the non-fluctuating target case. For fluctuating target cases, a fluctuation loss in dB is subtracted from D_0 in the iterative process. The general fluctuation loss for the five Swerling cases that are normally considered in radar systems is given by (Ref. 8, p.75).

$$L_f = \left[(-\ln P_d)(1+g_d/g_{fa})\right]^{-\frac{1}{K}} \qquad [83.]$$

where K is given by Table III. The Swerling case 3 is used when a missile-type target is considered. For large targets, like aircraft, the user can select either cases although a case 1 is recommended.

TABLE III

Parameter K of the chi-square family to describe the Swerling cases

TARGET MODEL	K
Non-fluctuating	$\rightarrow\infty$
Swerling I	1
Swerling II	N_e
Swerling III	2
Swerling IV	$2\,N_e$

6.5 Generation of Measurements

The generation of realistic "corrupted" measurements and the provision of the expected measurement error (to the tracking and data association algorithms) are needed for the data fusion analysis. Surveillance radars detect targets in space and report it in (R,θ) plane. The measurement errors indicate the accuracy of the radar output, while the resolution indicates the capability to resolve close targets. The measurement errors in range and azimuth depend on the quality of the received signal and thereby is a function of the target location. Simple relations between the measurement errors and *S/I* are provided in textbooks and are generally used in tracking studies.

The mean-range measurement error ε_R can be expressed as

$$\varepsilon_R = H_r \frac{C_R}{\sqrt{(S/I)_{out}}} \qquad [84.]$$

while for the mean angle measurement error ε_θ we have

$$\varepsilon_\theta = H_\theta \frac{\theta_b}{\sqrt{(S/I)_{out}}} \qquad [85.]$$

where C_R is the range cell and $(S/I)_{out}$ is the signal-to-interference ratio at the output of the threshold stage (Fig.2) (i.e. which includes the effect of the non-coherent integration). Usually, radar specifications give ε_R and ε_θ for a specific *S/I* ratio which allows to determine constants H_r and H_θ. When they are not supplied, $H_r = H_\theta$. = 4 is used as a default value. With this value, the mean error corresponds to the resolution when $(S/I)_{out}$ is 12 dB (a likely nominal detection threshold).

The measured target position is generated by adding random errors to the true-target position according to

$$R_{meas} = R_{true} + \mathrm{N}(0, f(\varepsilon_R)) \qquad [86.]$$

$$\theta_{meas} = \theta_{true} + \mathrm{N}(0, f(\varepsilon_\theta)) \qquad [87.]$$

where N is a Gaussian distribution with zero mean and with the variances taken to be

$$f(\varepsilon_R) = (\varepsilon_R/3)^2 \qquad [88.]$$

$$f(\varepsilon_\theta) = (\varepsilon_\theta/3)^2 \qquad [89.]$$

respectively, so that 99% of cases (plus-or-minus 3 times the standard-deviation) are within plus-or-minus the average value.

7.0 GENERATION OF FALSE ALARMS

For the study of sensor data correlation and fusion, generation of realistically spread out false alarms is as important as the predictions of detected target positions since the performance of fusion algorithms are to be assessed with respect to their capability of establishing target tracks out of false alarms.

Modern radar receivers include constant false alarm rate (CFAR) devices to adjust the detection threshold level so that P_{fa} remains constant in the presence of noise or interference. The need of CFAR arises when the noise level in the receiver varies with time in some unpredictable manner, when clutters are significant or in the presence of jamming. In the present radar model, we attempted to describe in a realistic manner the false alarm field caused by the system noise and sea clutter in the instrumental range-azimuth domain (R,θ) of the radar.

In the calculation of target P_d , P_{fa} is assumed to be kept constant in any circumstances at the cost of minor *S/I* losses, called CFAR losses. With the assumption of a constant false alarm rate, an increase of noise-like interferences results in a loss of detectability as the *S/I* decreases and the threshold increases.

False alarms caused by system noise occur at a rate corresponding to the mean time between false alarm t_{fa} which is directly related to P_{fa} (see Section 6.2). Section 7.1 describes the technique used to generate noise-induced false alarms.

Sea clutter can also be an important source of false alarms since CFAR systems can hardly adapt to the clutter statistical behavior which may substantially differ from that of Rayleigh noise. The density of sea-clutter false alarms depends on the radar characteristics (especially resolution, frequency, polarization), the environmental conditions (wind speed) and the grazing angle. The number of sea-clutter false alarms is normally much larger than the one due to noise. These false alarms are not uniformly

distributed in the (R,θ) domain. Their occurrence is expected to decrease with range (with decreasing grazing angle) and to increase in upwind direction.

The relationship between sea clutter false alarm probability, P_{fac} and the dependent factors is not sufficiently known to accurately predict P_{fac} versus range and azimuth for a diversity of radar characteristics and sea conditions. The literature essentially presents measurements of backscatter coefficient distribution for a limited set of environmental conditions and radar characteristics, and, furthermore, very little can be found on the capability radars to filter strong clutter returns. In spite of the incomplete knowledge on sea-clutter-induced false alarms, we deem that it is preferable to use a heuristic model that provides clutter-like spreading of false alarms rather than using a uniform spreading. The heuristic model of false alarm generation uses an approximative global false alarm rate that can be adjusted by the user and it features a spreading scheme which is representative of published experimental results.

7.1 Noise-Induced False Alarms

False alarms can occur in any of the N_{cells} resolution cells of the radar in the instrumental range-azimuth domain (R_{inst},θ), where

$$N_{cells} = \frac{360 R_{inst}}{\theta_b C_R} \qquad [90.]$$

- A detection is declared in a cell if the output of the signal processor for this cell exceeds a threshold. If the sensor points at a region where there is no target, then, detections can still occur due to noise with a probability given by P_{fa}. Assuming that the events in the cells are independent, the probability of having m false alarms in the (R_{inst},θ) domain is approximated, using $(\eta=N_{cells}P_{fa})$, by

- a Gaussian distribution with mean and variance equal to η, when $\eta \geq 9$;

$$f(n_{fa}=x)=\frac{1}{\sqrt{2\pi\eta}}\exp\left\{-\frac{(x-\eta)}{2\eta}\right\} \qquad [91.]$$

- a uniform distribution when $\eta<\frac{0.69}{2N_{ch}}$;

$$n_{fa}=\begin{cases}1 & U(0,1)\le\eta\\ 0 & otherwise\end{cases} \qquad [92.]$$

- otherwise, a Poisson distribution with mean η is used;

$$P(n_{fa}=m)=\frac{(\eta)^m\exp(-\eta)}{m!} \qquad [93.]$$

When generating the Poisson distribution, the "innovation filter" method, as described in Ref. 26, is used to determine the number of false alarms for each scan: n_{fa}. In this technique, the cumulative distribution (either Poisson or normal) is first evaluated. Then, a random number from 0 to 1 is drawn from a uniform distribution. The output n_{fa} is the number of event for which the cumulative probability corresponds to the drawn number. The last step consists in determining randomly n_{fa} positions in the (R,θ) domain using an uniform generator.

7.2 Sea-Clutter-Induced False Alarms

For sensor data fusion study, it is required to have a model that gives a realistic representation of the spreading of sea-clutter-induced false alarms as opposed to uniformly distributed false alarms. As our current knowledge on sea-clutter false alarms is not sufficient to achieve an accurate generation of false alarms as a function of the dependent factors (e.g. radar characteristics, environment), we essentially searched for a representative spatial variation of the sea-clutter-induced false alarm, P_{fac}, using likely values of global probabilities.

In the case of medium-to-high-resolution radars, sea-clutter amplitude distributions differ from the Rayleigh distribution; this is mainly due to the significant occurrence of

very large clutter returns, substantially larger than the mean backscatter coefficients σ_0 as calculated in Subsection 4.1.1. These large clutter returns, commonly referred to as *spikes*, are responsible for the formation of a longer tail in the backscatter distribution compared with Rayleigh distribution. Furthermore, spikes have been shown to have shifted and have larger spectrum than clutters of mean magnitudes (Ref. 16), which makes them even more difficult to be filtered out by radars.

Our model is based on the assumption that the CFAR devices are designed to adjust the threshold to obtain the required input P_{fa} assuming that clutters are Rayleigh distributed. Then, estimating the actual clutter distribution for a cell, one can compute the probability that clutters exceed the threshold for this cell. It is assumed that all returns greater than this threshold (hereafter called spikes) have the required magnitude and spectral content not to be filtered out by the radar clutter rejection stages.

The occurrence of spikes has been shown to increase with radar resolution and is thought to be negligible for low resolution radars. The data published in Ref. 10 (Fig. 7.14) and Refs. 16-17 suggest that non-Rayleigh distributions can be obtained for pulse lengths less than a few μs. Defining the product beamwidth-pulselength, X, as in Subsection 4.1.2, we can assume that spike-false alarms occur for $X < 4^{o}$-μs when the pulselength is shorter than 4 μs. Significant occurrences of spikes were observed by Chan (Ref. 16) in vertical polarization and Sekine et al. (Ref. 17) in horizontal polarization for X = 1 and 3.6^{o} μs, respectively. For greater X and pulselength values, clutter distribution becomes very close to Rayleigh's and so clutter-false alarms can be considered negligible.

Although it is now widely recognized that clutters are better characterized by a K-distribution (Ref. 16), Weibull distributions, being characterized by fewer parameters, are more convenient and they offer satisfactory performances (Refs. 16-18). In addition, the Weibull parameters can be related to physical conditions of operation. Using Weibull, the probability of clutter false alarms is the probability of having a return exceeding a threshold Y:

$$P_{fac} = P_{Weibull}(Y, a) = \exp\left(-\ln(2)\left(\frac{Y}{\sigma_{0median}}\right)^{Y_a}\right) \qquad [94.]$$

where a is the Weibull parameter and $\sigma_{0median}$ is the median backscatter coefficient. For a =1 the distribution reduces to Rayleigh's. In the calculation, the mean σ_0 (Subsection 4.1.1) is used in [94] instead of $\sigma_{0median}$.

Thence for any given sector of the (R,θ) domain, the probability of sea-clutter false alarm, P_{fac}, is calculated with [94] using σ_0 (mean) and a as given in the sea clutter table and the threshold Y_R,

$$Y_R = \sigma_{0median} + a_{\min}\left(10\log\left(\ln\left(1/P_{fa}\right)\right) + 1.6\right) \qquad [95.]$$

which corresponds to the required threshold to obtain P_{fac}= P_{fa} in the case of Rayleigh clutter (a_{min} = 1). Here again, the mean value σ_0 is used instead of the median value, $\sigma_{0median}$. The probability P_{fac} can then be evaluated for all sectors as defined in the clutter map. The technique described in Section 7.1 is then used to uniformly generate the false alarms in sectors from their respective P_{fac}.

Some authors (Ref. 15), show that the Weibull parameter a may be smaller than 1 (e.g. 0.8) at long ranges or for low mean backscatters. Consequently, we propose to let P_{fac} user-modifiable. At the same time, that gives the user a control of the global false alarm rate density. The parameter $a_{min,}$ is set to 1 and a new parameter $K_{clutter}$ is defined so that

$$P_{fac} = \frac{P_{Weibull}(Y, a)}{K_{clutter}} \qquad [96.]$$

where $K_{clutter}$ can be greater or equal to 1.

For sectors where a gets down to a_{min} or where the received sea-clutter power is of the order of the system noise ($2N_0'$ is arbitrary used), one can assume that sea clutter does behave like systems noise and so $P_{fa} = 0$ since the CFAR is assumed fully efficient in this case.

The false alarm generation technique hereabove described is based on clutter statistics which apply for vertical polarization (VP) exclusively, as they essentially describe the Bragg scatter component of clutters (Ref. 21). Unfortunately, the very few clutter data published so far in the literature in horizontal polarization (HP) prevent us to derive a similar false alarm generation technique for HP radar emissions. Although mean backscatters are weaker in HP, in general, distributions have longer tails, and, as shown by Chan (Ref. 16), the spike's spectrum in HP is shifted more, which suggests that, for a given threshold adjusted above the mean/median value, much greater P_{fac} would be obtained in HP than in VP.

Calculations performed using distributions published by Olin (Ref. 27) indicated that, in HP, the probability P_{fac} can be several orders of magnitude greater at sea state 2 and a bit less than 10 times greater at sea state 5 as compared with VP; these results agree with measurements published by Ewell (Ref. 28). Furthermore, in contrast with VP, in HP, P_{fac} is expected to slightly decrease with wind speed (and probably so with increasing mean backscatters); a decrease of P_{fac} of less than an order of magnitude can be predicted from sea state 2 to sea state 5 based on measurements published by Olin (Ref. 27).

Thence, in HP, the density of false alarms is not likely to decrease with range (and with the magnitude of mean backscatter) as fast as in VP. Furthermore, the global density of false alarms, which does not vary much with sea state, is expected to be significantly greater than in VP (likely to correspond about to the P_{fac} at very high sea state in VP in most cases). Consequently, in the simulation, until more information is found in the literature, for HP, we propose to use a relatively high maximum P_{facmax}, at close range (reference range corresponding to an angle of 3^o) for any wind speeds and to perform a

smooth decrease of P_{fac} up to the range where the parameter a reaches a_{min}, or where the received mean clutter power reaches $2N_0'$. At further ranges, P_{fac} is taken to be 0. For P_{facmax}, an arbitrary number between 10^{-2} and 10^{-3} can be selected by the simulation user or one can use the probability corresponding to $a = 3.0$ in VP.

The two histograms of Fig. 8 (a) and (b) show a comparison of the generation of noise-induced false alarms with clutter-induced false alarms. Arbitrary values were selected in order to highlight the behavior. In the case of noise (A) the false alarms are uniformily distributed in range while for clutter (B) the occurrence of false alarms rapidly decreases with range.

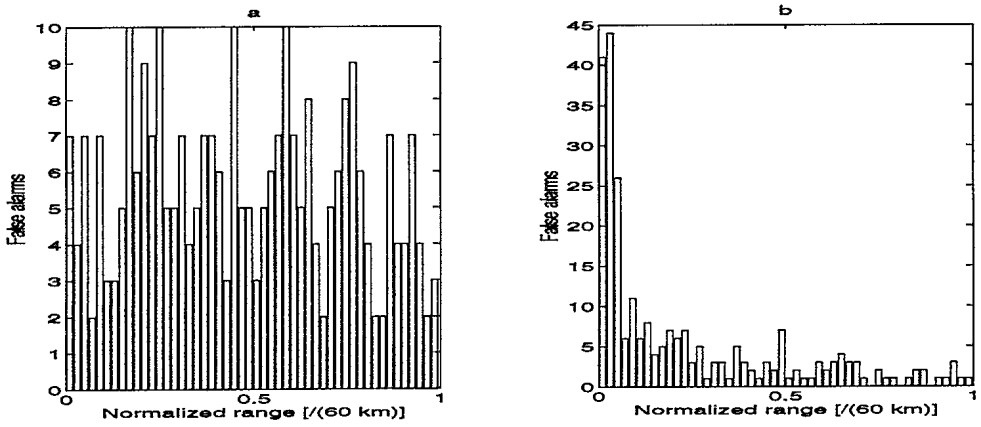

FIGURE 8 - An example of generation of false alarms (Histogram)
a) Noise-induced, b) Sea-clutter-induced

8.0 CONCLUSION

This document presented a model for the simulation of a surveillance radar for sensor data fusion studies. A panoramic pulse-MTI/Doppler search radar, typical of the Canadian Navy surveillance radars, using a rotating antenna that scans 360 degrees in azimuth was considered. The proposed model is more flexible and more generally applicable than the models published so far. It considers a wider range of parameters which affect a search or surveillance radar's performance; it is therefore likely to yield more "realistic" results. In particular, this model brings the following improvements:

- an extension to sea-clutter models to account for ducting;
- better identification of the various losses for a typical surveillance radar;
- full Parabolic Equation Method (PEM) computation of the propagation factor;
- a new model to generate false alarm measurements induced by sea clutter;
- a flexible and generic model to represent the effects of Doppler processing;
- a simulation architecture allowing refinement in modeling as well as real-time use for data fusion studies.

Most radar simulations have exclusively regarded the evaluation of target probability of detection in noise/clutter, and the current knowledge of the clutter process is not sufficiently advanced to provide accurate representation of clutter-produced false alarm outcomes. We have chosen therefore to use heuristic methods to achieve a more likely spreading of false alarms as a function of radar characteristics and environment. A probability of false alarms, P_{fac} was estimated as a function of range and azimuth.

A two-level processing architecture was proposed where the effects of environment and Doppler processing are precalculated and stored in tables: rain and sea clutter reflectivity tables, a propagation factor table, the Doppler processing improvement factor table and the probability of false alarms, P_{fac} table. Tables have to be precomputed

for the environmental conditions and radar characteristics for the cases of interest to be considered by CASE_ATTI.

The two-level processing architecture provides the flexibility of using various non-standardized pieces of software to precompute sensitive parameters without increasing complexity and therefore affecting the execution speed of the CASE_ATTI. Another advantage is that these external modules can be more conveniently upgraded as improved models become available. The model was particularly suited to data fusion studies where true and false measurements have to be generated while the scenario is running. True measurements are generated according to the P_d and the signal-to-interference ratio and false measurements are generated as a result of clutter and system noise.

This radar surveillance model is an important step towards the establishment of the CPF sensor suite baseline performance. Two radar sensors of the actual CPF sensor suite can be represented (SPS-49 and Sea Giraffe) by the model described in this report. This is needed to support the ongoing Multi-Sensor Data Fusion (MSDF) performance evaluation study in the CPF context

9.0 REFERENCES

1. Roy, J., Bossé, É., Dion, D., "CASE_ATTI: An Algorithm-Level Testbed for Multi-Sensor Data Fusion ", DREV-R-9411, May 1995, UNCLASSIFIED

2. Huizing, A.G. and Theil, A., " Computer-Aided Radar Performance Evaluation Tool: CARPET ", User's Manual, Artech House, N.Y., 1993.

3. Rohan, P., "Surveillance radar Prediction", Peter Peregrinus Ltd., N.Y., 1983.

4. Kaplan, D. J., Grindlay, A. and Davis, L., "Surveillance Radar Systems Evaluation Model (SURSEM) Handbook", Naval Research Laboratory, NRL Report No. 8037, Washington, D.C., 1977.

5. Craig, K.H. and Levy, M.F., "Parabolic Equation Modelling of the Effects of Multipath and Ducting on Radar Systems", IEE Proc. Part-F, 138 (2), pp. 153-162, April 1991.

6. Cayer, M., Philibert, B., Lecours, M. and Dion, D., "Analyse de la méthode Split-Step Fourier pour résoudre la propagation radio au-dessus de la mer", CCECE-Halifax, Université Laval, Vol. 2, pp. 421-424, 25-28 septembre , 1994.

7. Low, T.B. and Hudak, D.R., "Final Report on the Development and Testing of a Marine Boundary Layer Model", KelResearch Corp. Report , Contract No.W7701-8-2419/01-XSK, September 1990.

8. Blake, L.V., "Radar Range-Performance Analysis", Lexington Books, D.C. Heath and Company, Lexington, Massachusetts, 1982.

9. Beaulieu, A. J., Morley, G. and Roney, P., "The NAAWS IR Target Model (NIRTM-3) (U)", DREV R 4612/91, January 1991, SECRET

10. Nathanson, F.E., "Radar Design Principles", 2nd ed., McGraw-Hill, Inc., New York, 1990.

11. Horst, M. M., Dyer, F.B. and Tuley, M.T., "Radar Sea Clutter Model", Proc. IEE Int. Conf. Ant. and Prop., pp. 6-10, Nov. 1978.

12. Anderson, K.D., Barrios, A.E., Hattan, C.P., Hitney, Lindem, G.E., Patterson, W.L. and Paulus, R.A., "EREPS: Engineer's Refractive Effects Prediction System Software and User's Manual", Artech House, N.Y., 1990.

13. Dockery, G.D., "Method for Modelling Sea Surface Clutter in Complicated Propagation Environments", IEE Proc., Vol. 137F, No. 2, pp. 73-79, April 1990.

14. Helmken, H.F., "Low-Grazing Angle Radar Backscatter form the Ocean Surface", IEE Proc., Vol. 137F, No. 2, pp. 113-117, April 1990.

15. Dyer, F.B. and Currie, N. C., "Some Comments on the Characterization of Radar Sea Clutter", IEEE Int. Symp. on Ant. and Prop., pp. 323-326, 1974.

16. Chan, H.C., "Radar Sea-Clutter at Low Grazing Angles", IEE Proc., Vol. 137F, No. 2, pp. 102-112, April 1990.

17. Sekine, M., Musha, T., Tomita, Y., Hagisawa, T., Irabu, T. and Kiuchi, O., "Weibull Distributed Sea Clutter", IEE Proc., Vol. 130F, p. 476, 1983.

18. Sekine, M. and Mao, Y., "Weibull Radar Clutter", Peter Peregrinus Ltd., Stevenage, UK, 1990.

19. Trizna, D.B., "Open Ocean Radar Sea Scatter Measurements", IEEE 1985 Int. Radar Conf., pp.135-140, May 1985.

20. Fay, F.A., Clarke, J. and Peters, R.S., "Weibull Distribution Applied to Sea Clutter", IEE Int. Conf. Radar '77, pp. 101-104, 1977.

21. Trizna, D.B., Hansen, J.P., Hwang, P. and Wu, J., "Laboratory Studies of Radar Sea Spikes at Low Grazing Angles", Journal of Geophysical Research, Vol. 96, No. C7, pp. 12529-12537, July 1991.

22. Hsiao, J. K., "On the Optimization of MTI Clutter Rejection", IEEE Trans. on AES, Vol. AES-10, No.5, pp. 622-629, Sept. 1974.

23. Harris, F. J., "On the Use of Windows for Harmonic Analysis with the Discrete Fourier Transform", Proc. IEEE, Vol. 66, No.1, Jan. 1978.

24. Schleher, D.C., "MTI detection loss in clutter", Electron. Letts., Vol. 17, pp. 82-83, 1981.

25. Trunk, G.V., "MTI Noise Integration Loss", Proc. IEEE, Vol. 65, No. 11, pp. 1620-1621, Nov. 1977.

26. Papoulis, A., "Probability, Random Variables and Stochastic Processes", 4th ed., McGraw Hill, NY, 1984.

27. Olin, I.D., "Amplitude and Temporal Statistics of Sea Spike Clutter", IEE Int. Conf. Radar '82, pp. 198-202, Oct. 1982.

28. Ewell, G.W., Tuley, M.T. and Horne, W.F., "Temporal and Spatial Behavior of High Resolution Sea Clutter 'Spikes'", IEEE 1984 National Radar Conf., 1984, pp. 100-104, April 1984.

INTERNAL DISTRIBUTION

DREV - R - 9429

1 - Deputy Director General
1 - Director Command, Control and Information Systems Division
1 - Director Electro-Optics and Surveillance Division
6 - Document Library
1 - É. Bossé (author)
1 - D. Dion (author)
1 - J.M.J. Roy (author)
1 - G. Picard
1 - R. Larose
1 - G. Otis
1 - J. Berger
1 - R. Carling
1 - B. Chalmers
1 - V. Larochelle

EXTERNAL DISTRIBUTION

DREV - R - 9429

2 - DSIS
1 - CRAD
1 - DMCS
1 - DMCS - 2
1 - DMCS - 4
1 - DMCS - 4 - 3
1 - DMCS - 4 - 3 - 6
1 - DMCS - 4 - 4
1 - DMCS - 4 - 4 - 3
1 - DMCS - 7
1 - DMCS - 7 - 3
1 - DMCS - 7 - 3 - 2
1 - DMCS - 7 - 7
1 - DMCS - 7 - 7 - 2
1 - DMFD
1 - DMOR
1 - DNR
1 - DNR - 3 - 5
1 - DRDCS
1 - DRDM
1 - DRDM - 6
1 - DRDM - 11
4 - DREO
Attn: D. Liang
H.C. Chan
B. Wong
P. Yansouni

EXTERNAL DISTRIBUTION (continued)

DREV - R - 9429

1 - PMO CPF

2 - CF Maritime Warfare School
CFB Halifax
Halifax, Nova Scotia
Attn: LCDR Connor
LCDR Harrison

2 - Department of Electrical Engineering
Laval University
Ste-Foy, Quebec
G1K 7P4
Attn: D. Grenier
M. Lecours

2 - Communication Research Laboratory
McMaster University
1280 Main Street West
Hamilton, Ontario
L8S 4L7
Attn: J. Litva
M. Wong

4 - Groupe INFORMISSION inc.
2014, Boul. Charest Ouest
Bureau 109, Ste-Foy
Québec, G1N 4N6
Attn: N. Duclos-Hindié
M. Mercier
J. Audet

1 - Loral Canada Inc.
6111, avenue Royalmount
Montréal, Québec
H4P 1K6
Attn: E. Shahbazian

UNCLASSIFIED
SECURITY CLASSIFICATION OF FORM
(Highest classification of Title, Abstract, Keywords)

DOCUMENT CONTROL DATA

1. ORIGINATOR (name and address) DREV 2459 Blvd Pie XI North P.O. Box 8800 Courcelette, Qc G0A 1R0	2. SECURITY CLASSIFICATION (Including special warning terms if applicable) UNCLASSIFIED

3. TITLE (Its classification should be indicated by the appropriate abbreviation (S,C,R or U)

"A SHIPBORNE SURVEILLANCE RADAR MODEL FOR DATA FUSION STUDIES" (U)

4. AUTHORS (Last name, first name, middle initial. If military, show rank, e.g. Doe, Maj. John E.)

BOSSÉ, Éloi, DION, Denis and ROY, Jean

5. DATE OF PUBLICATION (month and year)	6a. NO. OF PAGES	6b. NO. OF REFERENCES
November 1995	66	28

7. DESCRIPTIVE NOTES (the category of the document, e.g. technical report, technical note or memorandum. Give the inclusive dates when a specific reporting period is covered.)

Report

8. SPONSORING ACTIVITY (name and address)

N/A

9a. PROJECT OR GRANT NO. (Please specify whether project or grant)	9b. CONTRACT NO.
0112C14A (Sensor Data Fusion)	N/A
10a.ORIGINATOR'S DOCUMENT NUMBER	**10b. OTHER DOCUMENT NOS.**
DREV-R-9429	N/A

11. DOCUMENT AVAILABILITY (any limitations on further dissemination of the document, other than those imposed by security classification)

- [X] Unlimited distribution
- [ ] Contractors in appoved countries (specify)
- [ ] Canadian contractors (with need-to-know)
- [ ] Government (with need-to-know)
- [ ] Defence departments
- [ ] Other (please specify) :

12. DOCUMENT ANNOUNCEMENT (any limitation to the bibliographic announcement of this document. This will normally correspond to the Document Availability (11). However, where further distribution (beyond the audience specified in 11) is possible, a wider announcement audience may be selected.)

Unlimited announcement

UNCLASSIFIED
SECURITY CLASSIFICATION OF FORM

UNCLASSIFIED
SECURITY CLASSIFICATION OF FORM

13. ABSTRACT (a brief and factual summary of the document. It may also appear elsewhere in the body of the document itself. It is highly desirable that the abstract of classified documents be unclassified. Each paragraph of the abstract shall begin with an indication of the security classification of the information in the paragraph (unless the document itself is unclassified) represented as (S), (C), (R), or (U). It is not necessary to include here abstracts in both official languages unless the text is bilingual).

This report presents a surveillance radar model to support the ongoing multi-sensor data fusion performance evaluation study for potential application to the Canadian Patrol Frigate midlife upgrade. This surveillance radar model takes into account the sensor's design parameters and external environmental effects such as clutter, propagation and jamming. To a large extent, the model is based on the available literature and on relevant experience and recent studies in the field. In addition, the latest findings regarding the dominant perturbing effects affecting the radar detection performance are included. The radar model can be used to generate contacts and false alarms in scenarios for multi-sensor data fusion studies while the scenario is running.

14. KEYWORDS, DESCRIPTORS or IDENTIFIERS (technically meaningful terms or short phrases that characterize a document and could be helpful in cataloguing the document. They should be selected so that no security classification is required. Identifiers, such as equipment model designation, trade name, military project code name, geographic location may also be included. If possible keywords should be selected from a published thesaurus. e.g. Thesaurus of Engineering and Scientific Terms (TEST) and that thesaurus-identified. If it is not possible to select indexing terms which are Unclassified, the calssification of each sould be indicated as with the title.)

Radar model simulation
Radar detection
Sensor Data Fusion
Performance Evaluation Methodology

154344

UNCLASSIFIED
SECURITY CLASSIFICATION OF FORM